HHS Public Access

Author manuscript

Sci Transl Med. Author manuscript; available in PMC 2024 July 31.

Published in final edited form as:

Sci Transl Med. 2024 January 31; 16(732): eadg7895. doi:10.1126/scitranslmed.adg7895.

Myeloid and lymphoid expression of *C9orf72* regulates IL-17A signaling in mice

Francesco Limone[1,2,3,4,‡], **Alexander Couto**[1,2,3,‡], **Jin-Yuan Wang**[1,2,3], **Yingying Zhang**[1,2,3], **Blake McCourt**[5], **Cerianne Huang**[5], **Adina Minkin**[5], **Marghi Jani**[5], **Sarah McNeer**[5], **James Keaney**[6], **Gaëlle Gillet**[6], **Rodrigo Lopez Gonzalez**[7], **Wendy A. Goodman**[5], **Irena Kadiu**[6], **Kevin Eggan**[1,2,3,*], **Aaron Burberry**[1,2,3,5,*]

[1.]Department of Stem Cell and Regenerative Biology, Harvard University, Cambridge, MA, 02138, USA

[2.]Stanley Center for Psychiatric Research, Broad Institute of MIT and Harvard, Cambridge, MA, 02142, USA

[3.]Harvard Stem Cell Institute, Harvard University, Cambridge, MA, 02138, USA

[4.]Leiden University Medical Center, LUMC, 2333 ZA Leiden, The Netherlands

[5.]Department of Pathology, Case Western Reserve University, Cleveland, OH, 44106, USA

[6.]Neuroinflammation Focus Area, UCB Biopharma SRL, Braine-l'Alleud, 1420, Belgium

[7.]Department of Neurosciences, Lerner Research Institute, Cleveland Clinic, Cleveland, OH, 44196, USA

Abstract

A mutation in *C9ORF72* is the most common cause of Amyotrophic Lateral Sclerosis (ALS) and Frontotemporal Dementia (FTD). Patients with ALS or FTD often develop autoimmunity and inflammation that precedes or coincides with the onset of neurological symptoms, but the underlying mechanisms are poorly understood. Here, we knocked out murine *C9orf72* in seven hematopoietic progenitor compartments by conditional mutagenesis and found that myeloid lineage *C9orf72* prevents splenomegaly, loss of tolerance, and premature mortality. Furthermore,

[*]Corresponding authors: aaron.burberry@case.edu and kevin.eggan@bmrn.com.
[‡]These authors contributed equally

Author contributions:

A.B. and K.E. conceptualized the studies. Spleen and CNS mass cytometry was conducted by F.L., J.K, G.G, I.K, A.C., J.Y.W., and Y.Z. Spleen and CNS RNA sequencing studies were conducted by F.L. and J.Y.W. Auto-antibody analysis was conducted by C.H. Mouse tissue immunophenotyping was conducted by Y.Z., A.C., B.M., C.H., A.M., M.J., S.M., and W.A.G. T cell analysis was conducted by S.M. and W.A.G. In vitro macrophage studies were conducted by B.M., A.M., and M.J. Mouse survival studies were conducted by A.C. The anti-IL17A experiment was conducted by A.C. R.L.G conducted the human IHC experiment. A.B. conducted mouse survival studies, conditional mutant mouse tissue immunophenotyping and plasma and autoantibody analysis, spleen and CNS mass cytometry, human IHC experiment, macrophage protein and flow cytometry and immunofluorescence analysis, CNS and spleen RNA sequencing analysis, Il-17a LOF mouse immunophenotyping, T cell analysis and autoantibody analysis, anti-IL-17A experiment and fecal DNA PCR. A.B. and F.L. visualized data; A.B., F.L., W.A.G., and K.E. wrote the original manuscript draft; A.B., F.L., W.A.G., and K.E. performed review and editing.

Competing interests: K.E. is a founder of Q-State Biosciences, QurAlis, and EnClear Therapies, and is employed at BioMarin Pharmaceutical. G.G. and I.K. are employed at UCB Biopharma SPRL. J.K. is a former employee of UCB Biopharma SPRL and is currently employed at F. Hoffmann-LaRoche. J.Y.W. is currently affiliated with STEMCELL Technologies Inc. AG. A.B and K.E. are authors on a pending patent that describes methods for suppressing inflammation induced by gut microbes (WO/2021/231804). All other authors declare they have no conflict of interest.

we demonstrated that *C9orf72* plays a synergistic role in lymphoid cells to prevent interleukin (IL)-17A production and neutrophilia. Mass cytometry identified early and sustained elevation of the co-stimulatory molecule CD80 expressed on *C9orf72*-deficient mouse macrophages, monocytes, and microglia. Enrichment of CD80 was similarly observed in human spinal cord microglia from patients with *C9ORF72*-mediated ALS compared with non-ALS controls. Single cell RNA sequencing of murine spinal cord, brain cortex, and spleen demonstrated coordinated induction of gene modules related to antigen processing and presentation and antiviral immunity in *C9orf72*-deficient endothelial cells, microglia, and macrophages. Mechanistically, C9ORF72 repressed the trafficking of CD80 to the cell surface in response to toll-like receptor agonists, interferon-γ, and IL-17A. Deletion of *Il17a* in *C9orf72*-deficient mice prevented CD80 enrichment in the spinal cord, reduced neutrophilia, and reduced gut T helper type 17 cells. Lastly, systemic delivery of an IL-17A neutralizing antibody augmented motor performance and suppressed neuroinflammation in *C9orf72*-deficient mice. Altogether, we show that *C9orf72* orchestrates myeloid co-stimulatory potency and provides support for IL-17A as a therapeutic target in ALS/FTD.

One Sentence Summary:

The ALS-associated *C9orf72* gene product opposes IL-17A-dependent inflammation in myeloid and lymphoid cells.

Editor's Summary:

C9ORF72 is commonly mutated in Amyotrophic Lateral Sclerosis (ALS) and Frontotemporal Dementia (FTD) and loss of function has been associated with autoimmune inflammation. Limone *et al.* find that hematopoietic loss of *C9orf72* expression drives excess IL-17A inflammation, whereas loss of *C9orf72* in myeloid cells is sufficient to cause severe autoimmunity. *C9orf72* deficient mice had more myeloid cells with high surface expression of co-stimulatory molecule CD80 which was potentiated by IL-17A. Patients with *C9ORF72*-related ALS similarly showed enrichment of CD80 in spinal cord microglia. IL-17A neutralizing antibody therapy in *C9orf72* deficient mice reduced neuroinflammation and support further investigation of IL-17A-based therapies for ALS or FTD. –Molly Ogle

INTRODUCTION

The most common inherited cause of amyotrophic lateral sclerosis (ALS) and frontotemporal dementia (FTD) is a hexanucleotide (GGGGCC) repeat expansion within the first intron of *Chromosome 9 Open Reading Frame 72 (C9ORF72)*. The mutation accounts for 20-40% of familial ALS cases and 2-8% of sporadic ALS cases and is enriched in people of European descent (1). The mutation is transcribed into long repetitive ribonucleic acid (RNA) species and undergoes repeat associated non-AUG translation into dipeptides, both of which can produce toxic gain-of-function (GOF) effects when overexpressed in the central nervous system or in cultured neurons (2–4). Independent of these gain-of-function (GOF) effects, epigenetic repression and failure of RNA polymerase to read through the mutation in brain and hematopoietic cells leads to a loss-of-function (LOF) mechanism and reduction of the gene normally encoded at the *C9ORF72* locus (5).

C9ORF72 exhibits GTPase activating protein (GAP) activity towards small GTPases of the RAB and ARF family that function as molecular switches to mediate vesicle trafficking, actin cytoskeletal rearrangement, and autophagic flux (6–9). In mice, the *C9ORF72* ortholog (*C9orf72*) suppresses age-related inflammation and autoimmunity, as well as promoting phagolysosomal clearance of dipeptides to restrain GOF toxicities of a transgene-encoded *C9ORF72* repeat expansion (10–15). A key question is whether and how *C9ORF72* LOF-driven peripheral autoimmunity imparts risk of motor neuron disease.

Chronic inflammation may be a contributor to ALS (16), as autoimmune diseases often precede an ALS/FTD diagnosis (17, 18) and neuroinflammation at disease onset correlates with the rate of motor decline (19, 20). The ratio of circulating T helper type 17 (Th17) to T regulatory cells (T_{reg}) cells is elevated in patients with ALS who experience a rapid disease course (21) which supports a role for adaptive immune cells in disease progression. Interleukin (IL)-17A , a key proinflammatory cytokine produced by Th17 cells and elevated in many auto-inflammatory disorders (22), is elevated in ALS/FTD plasma and cerebral spinal fluid, including in patients with a *C9ORF72* mutation (23–26). However, the extent to which GOF or LOF sequelae of the *C9ORF72* mutation contribute to inflammation, autoimmunity, and neural degeneration in patients with ALS and FTD, as well as the relative importance of the IL-17A inflammatory axis, remains incompletely understood.

Therapeutic efforts to restore *C9ORF72* function in ALS/FTD patients will benefit from the knowledge of cell types and pathways in which this gene acts to promote organismal health. However, *C9ORF72* cellular function remains poorly understood, in part because the gene is widely expressed in all three germ layers. The profound inflammatory response that manifests in *C9orf72* LOF mice (10–13) has prompted investigation into whether this gene product serves an important function in the immune system. Reciprocal bone marrow transplantations established that *C9orf72* is required in both radio-sensitive and radio-resistant cells to oppose systemic inflammation and fatal autoimmunity (11). Studies in which *C9orf72*-deficient mice that were reared in different environments, treated with antibiotics, or received fecal transplant showed that neuroinflammation and fatal autoimmune disease occur in response to signals derived from gut bacteria (27). *C9orf72* acts in macrophages to suppress the release of inflammatory cytokines when exposed to gut bacteria (27) implicating the innate immune response as a governor of organismal disease severity. Furthermore, selective depletion of *C9orf72* within *Cx3cr1*- or *LysM*-expressing cells in mice caused inflammation that was dependent on the cytosolic DNA sensor Stimulator of interferon genes (STING) (28). However, because spontaneous autoimmune disease was not reported in *C9orf72*-deficient or myeloid conditional mutant mice reared in that environment (28), it has remained unclear whether the function of *C9orf72* in myeloid cells is required to maintain immune tolerance and to what extent, if any, *C9orf72* functions in other hematopoietic lineages to oppose systemic and nervous system inflammation.

Here, we have addressed this knowledge gap by performing a conditional mutagenesis screen of *C9orf72* activity across discrete hematopoietic lineages and by profiling gene expression and protein abundance of *C9orf72* LOF mice with single-cell resolution. Targeted mutagenesis confirmed a general role for *C9orf72* in the hematopoietic system and a specific role in myeloid cells and lymphoid cells to oppose systemic inflammation and

autoimmunity. We found that *C9orf72*-deficient microglia and endothelial cells participate in a coordinated induction of neuroinflammation that is characterized by dynamic activation of antigen processing and presentation, cytokine production, and antiviral immunity. Further delineating the function of C9ORF72, we identify *Il-17a*-dependent accumulation of the potent co-stimulatory molecule CD80 on the surface of *C9orf72*-deficient macrophages, microglia, and brain-infiltrating monocytes and demonstrate therapeutic improvement of motor function and neuroinflammation with IL-17A neutralization. Collectively, our findings identify roles for *C9orf72* in both lymphoid and myeloid lineages, where it confers protection against pathogenic Th17-associated inflammation and maintains neural health.

RESULTS

Myeloid lineage-expressed *C9orf72* restrains autoimmune inflammation and supports a normal lifespan.

C9ORF72 and its murine ortholog are enriched in monocytes, granulocytes, erythrocytes, dendritic cells, B cells, and activated T cells (fig. S1, A and B) (29). Our previous bone marrow transplant studies suggested a potential role for *C9orf72* in the hematopoietic system to oppose fatal autoimmunity (11). To test the hypothesis that *C9orf72* promotes organismal health by acting in divergent blood lineages, we crossed mice carrying two copies of a floxed *C9orf72* (*C9orf72*$^{2Lox/2Lox}$) allele (30) with seven different Cre recombinase lines to generate cohorts of conditional knockout mice (*C9orf72*$^{2Lox/2Lox}$ Cre+) and littermate controls (*C9orf72*$^{2Lox/2Lox}$ Cre−) for study (Fig. 1, A and B and fig. S1C). Vav guanine nucleotide exchange factor 1 (*Vav1*)-Cre and poly(I:C) induced MX dynamin-like GTPase 1 (*Mx1*)-Cre serve as positive controls for the depletion of *C9orf72* within all hematopoietic cells (31, 32). Lysozyme 2 (*LysM*)-Cre was used to inactivate *C9orf72* broadly in the myeloid lineage (33), whereas *CD2*-Cre was chosen to deplete *C9orf72* in common lymphoid progenitors (34). Additionally, we targeted *C9orf72* for depletion within CD19$^+$ B cells (*CD19*-Cre) (35), CD4$^+$ and CD8$^+$ T cells (*CD4*-Cre) (36), and Forkhead box P3 (FoxP3$^+$) T_{reg} cells (*Foxp3*-Cre) (Fig. 1B) (37). For each intercross, the presence of Cre recombinase was associated with a reduction in the size of the *C9orf72* locus (fig. S1D). *C9orf72* expression was completely abrogated in peripheral blood from *C9orf72*$^{2Lox/2Lox}$;*Vav1*-Cre+ mice (fig. S1E) and *C9orf72* was selectively depleted in sorted CD11c$^+$ dendritic cells (DCs) and F4/80$^+$ macrophages, but not B cells or neutrophils, in *C9orf72*$^{2Lox/2Lox}$;*LysM*-Cre+ mice (fig. S1F and table S1) as expected.

Complete knockout of *C9orf72* in mice (*C9orf72*$^{-/-}$) is characterized by splenomegaly as an early and sensitive indicator of inflammatory disease progression (10–15). Hematopoietic cell and myeloid lineage-specific conditional knockouts (*C9orf72*$^{2Lox/2Lox}$;*Vav1*-Cre+, *Mx1*-Cre+, and *LysM*-Cre+ mice) exhibited splenomegaly relative to littermate Cre− controls, but spleen weight was not altered in the lymphoid-specific Cre+ lines studied (Fig. 1, C and D). *C9orf72*$^{-/-}$ mice experience premature death (Fig. 1E, **red line**), therefore, to test whether myeloid lineage conditional deletion of *C9orf72* was sufficient to cause premature death, we aged a cohort of *C9orf72*$^{2Lox/2Lox}$;*LysM*-Cre+ (n=16) and *LysM*-Cre− control littermates (n=9) to 600 days and compared their survival to other *C9orf72*$^{+/+}$ (n=869) and *C9orf72*$^{-/-}$ (n=838) mice that were reared contemporaneously

(Fig. 1E). All control *C9orf72*$^{2Lox/2Lox}$;*LysM*-Cre− mice survived beyond 500 days of age (781-day median survival) and their survival did not differ from *C9orf72*$^{+/+}$ controls (Fig. 1E). *C9orf72*$^{2Lox/2Lox}$;*LysM*-Cre+ animals (547-day median survival) died significantly faster than *LysM*-Cre− controls ($p = 0.0252$) (Fig. 1E), whereas *C9orf72*$^{2Lox/2Lox}$;*LysM*-Cre+ mice lived significantly longer than *C9orf72*$^{-/-}$ mice (462-day median survival) ($p = 0.0481$) (Fig. 1E). Male *C9orf72*$^{-/-}$ (439-day median survival) tended to have a shorter median survival time than female *C9orf72*$^{-/-}$ mice (499-day median survival) ($p < 0.0001$), but the *C9orf72*$^{2Lox/2Lox}$;*LysM*-Cre+ cohort was not sufficiently powered to assess differences between sexes (fig S1G). The *C9orf72*$^{2Lox/2Lox}$;*LysM*-Cre+ animals exhibited wasting, hepatomegaly, and labored breathing, which were also commonly displayed by *C9orf72*$^{+/-}$ and *C9orf72*$^{-/-}$ mice (11). These results indicate that myeloid *C9orf72* prevents splenomegaly, a feature of systemic inflammation, and promotes a longer lifespan.

C9orf72 acts in diverse blood lineages to prevent autoimmunity.

Because depletion of *C9orf72* in the myeloid lineage (*LysM*-Cre) caused premature mortality with delayed kinetics relative to *C9orf72*$^{-/-}$ mice, we reasoned that our conditional mutagenesis survey could yield insight into the epistasis of inflammatory and autoimmune phenotypes that develop upon loss of *C9orf72* (11). Consistent with a necessary role for *C9orf72* in hematopoietic cells, *C9orf72*$^{2Lox/2Lox}$;*Vav1*-Cre+ animals recapitulated the autoinflammatory phenotype of *C9orf72*$^{-/-}$ mice. *Vav1*-Cre+ mice had elevated plasma IgM and IgG autoantibodies (Fig. 1F and fig. S2, A and B), decreased circulating platelets indicative of pseudothrombocytopenia, a phenomena caused by autoantibodies that aggregate platelets, (Fig. 1G) (27) and neutrophilia (Fig. 1H). Cytokines and chemokines significantly ($p < 0.05$) elevated in *C9orf72*$^{2Lox/2Lox}$;*Vav1*-Cre+ plasma included IL-17A, IL-23, IL-6, IL-22, IL-15/15R, IL-3, IL-31, CXCL1 (GRO-α), CCL2 (Mcp1), and IL-28 (Fig. 1I). Conditional depletion of *C9orf72* within either the myeloid (*LysM*-Cre+) or lymphoid (*CD2*-Cre+) lineage was sufficient to cause autoimmune phenotypes characterized by increased autoantibodies in plasma (Fig. 1, F and G), but did not lead to systemic elevation of cytokines or neutrophilia (Fig. 1, H and I). Reduction of *C9orf72* in B cells or T cells alone did not cause detectable immune phenotypes (Fig. 1, C to I). Although IgG autoantibodies did not differ appreciably upon myeloid *C9orf72* depletion, the IgM autoantibodies that were elevated in *C9orf72*$^{2Lox/2Lox}$;*LysM*-Cre+ and *C9orf72*$^{2Lox/2Lox}$;*Mx1*-Cre+ mice targeted proteins important for blood brain barrier integrity (Aquaporin 4, Vitronectin, Elastin, Collagen IV) (38–40) and microglia- and astrocyte-mediated synaptic pruning by the complement cascade (C9, C3, C4, C1q, Factor H) (fig. S2A) (41). Taken together, our results indicate that *C9orf72* functions separately in myeloid and lymphoid lineages to promote immunological tolerance and cooperatively in these lineages to prevent systemic elevation of IL-17-related inflammatory cytokines and neutrophils (Fig.1J).

C9orf72 deficiency alters immune cell surface effector protein abundance.

We next sought to identify *C9orf72*-regulated factors that underlie pathogenesis in this model. We reasoned that deep immunophenotyping of the spleen might yield mechanistic insight because resident professional antigen-presenting cells (APCs) such as macrophages and DCs integrate signals from the environment, display foreign and self-antigens on their cell surface, and provide signals that govern the activity of T cells (42). A panel of 34 heavy

isotope-labeled antibodies was designed that included 16 antigens to assign cellular identity and 18 functional effectors with a focus on interactions between APCs and T cells (Fig. 2A and table S2).

The abundance of different lineages among splenocytes was analyzed by mass cytometry from 2- or 8-month-old mice in *C9orf72*$^{+/+}$ or *C9orf72*$^{-/-}$ (Fig. 2B). We identified nine unique cell types based on their cell surface marker expression (Fig. 2, C and D and fig. S3, A to H). At 2 months of age, *C9orf72*$^{-/-}$ mice displayed a significant accumulation of CD8^{+} DCs ($p = 0.0040$), CD8^{-} DCs ($p = 0.0043$), monocytes ($p < 0.0001$), neutrophils ($p < 0.0001$) and B cells ($p = 0.0243$) (Fig. 2D). By 8 months of age, *C9orf72*$^{-/-}$ maintained these elevated cell populations and also displayed an increase in macrophages ($p = 0.0214$) and CD4^{+} T cells ($p = 0.0005$) (Fig. 2D). Thus, *C9orf72* deficiency caused changes in multi-lineage hematopoiesis (11).

Next, we quantified the median staining intensity of each surface effector in the nine gated populations and performed a Bonferroni-corrected two-tailed t-test or Mann-Whitney test for non-normal distributions with significance threshold set to $p < 0.0056$ (0.05 divided by 9 to correct for multiple comparisons). This analysis revealed 44 significant differences between *C9orf72*$^{-/-}$ and control populations at 2 months of age and 51 significant differences at 8 months of age ($p < 0.0056$) (Fig. 2E and fig. S3F). Increased surface expression of the high-affinity F_c γ Receptor (CD64) on *C9orf72*$^{-/-}$ macrophages, CD8^{-} DCs, and monocytes, but not neutrophils (Fig. 2E), was consistent with development of autoimmune disease rather than acute bacterial infection in these animals (43). Surface expression of the chemokine receptor CXCR4 and hyaluronan receptor CD44, both involved in homing to sites of inflammation, were increased on multiple *C9orf72*$^{-/-}$ populations (fig. S3F). Macrophages from *C9orf72*$^{-/-}$ mice displayed a significant elevation in the surface expression of CD83 ($p < 0.0056$) (Fig. 2E), a molecule that is highly expressed in monocytes from patients with ALS with a rapid disease course (44). Additionally, *C9orf72*$^{-/-}$ macrophages showed elevation of the immune checkpoint receptors leukocyte immunoglobulin-like receptor subfamily member 4 (LILRB4/CD85k) and Signal-regulatory protein α (SIRPα/CD172A), the immunosuppressive ectonucleotidase CD39, and the scavenger receptor CD48 (Fig. 2E). Together, these data suggest that the overall profile of *C9orf72*$^{-/-}$ APCs is biased towards a pro-inflammatory state and that the balance of inhibitory molecules may govern the extent of disease in each mutant animal.

C9orf72 restricts co-stimulatory potential of myeloid cells in the periphery and central nervous system (CNS).

Naïve T cells require two signals to initiate a self-reactive inflammatory response. The first signal is provided by the interaction of the T cell receptor with a self-antigen that is displayed within the major histocompatibility complex (MHC) of APCs, whereas a second co-stimulatory signal licenses T cells to repeatedly proliferate (45). We found no difference in the abundance of MHC class I (H-2D^{b}/H-2L^{d}/H-2D^{q}/H-2L^{q}) or MHC class II (I-A/I-E) on the surface of *C9orf72*$^{-/-}$ APCs relative to controls (Fig. 2E and fig. S3F). However, the co-stimulatory molecule CD80 was prominently enriched on the surface *C9orf72*$^{-/-}$ macrophages and CD8^{+} DCs at 2 months of age and persisted on *C9orf72*$^{-/-}$ macrophages at

8 months of age (Fig. 2E). The co-stimulatory molecule CD86 was consistently enriched on the surface of *C9orf72*$^{-/-}$ CD8^{-} DCs, and the CD40 co-stimulatory molecule was enriched on *C9orf72*$^{-/-}$ CD8^{+} DCs at 2 months of age (Fig. 2E).

Given that inflammatory phenotypes depend on the gut microbiota in this model (27), we interrogated co-stimulatory molecule expression on immune cells isolated from the colon, Peyer's patch, mesenteric lymph node (mLN), and spleen of *C9orf72*$^{+/+}$ and *C9orf72*$^{-/-}$ mice. Relative to *C9orf72*$^{+/+}$ controls, we observed a 54-fold enrichment of CD80^{hi} CD11b^{+} cells in the spleen ($p = 0.0298$) and 23-fold enrichment of CD80^{hi} CD11b^{+} cells in mLNs ($p = 0.0042$) of *C9orf72*$^{-/-}$ mice, respectively, whereas no differences were observed in Peyer's patch- or colon-derived myeloid cells (Fig. 2, F and G). To test the functional co-stimulatory potential of APCs, we treated tissue resident macrophages from *C9orf72*$^{-/-}$ and *C9orf72*$^{+/+}$ mice with $OVA_{323-339}$ peptide in co-culture with OTII CD4^{+} T cells. Enrichment of CD80 on *C9orf72*$^{-/-}$ macrophages from spleens and mLNs was associated with enhanced ability to promote antigen specific T cell proliferation (Fig. 2H).

We next asked whether co-stimulation was altered in the CNS of *C9orf72* LOF mice. Evaluation of mass cytometry performed on forebrain and spinal cord of 8-month-old *C9orf72*$^{+/+}$, *C9orf72*$^{+/-}$, and *C9orf72*$^{-/-}$ mice revealed significant accumulation of CD80^{hi} microglia in the forebrain and CD80^{hi} monocytes in the forebrain and spinal cord of *C9orf72*$^{-/-}$ mice relative to *C9orf72*$^{+/+}$ controls ($p < 0.05$) (Fig. 3, A and B). No enrichment of CD80 was observed in *C9orf72*$^{+/-}$ CNS or periphery (Fig. 3, A and B and fig. S3G). MHC-II^{hi} myeloid cells were elevated in *C9orf72*$^{-/-}$ forebrain and spinal cord, however, CD86, CD40, and MHC I did not differ between genotypes (fig. S4A). Thus, *C9orf72* restrains myeloid co-stimulation in the brain and secondary lymphoid organs, where CD80 may enhance antigen-specific helper T cell responses.

Human *C9ORF72* ALS microglia accumulate CD80.

To determine whether high CD80 expression was a conserved feature in ALS, we stained human spinal cord from *C9ORF72* ALS cases (n=4) and non-ALS controls (n=3) for CD80 and imaged more than 440 Iba1^{+} microglia per case (Fig. 3C). We observed significantly greater CD80 staining on *C9ORF72* ALS spinal cord microglia relative to non-ALS microglia ($p = 0.0199$) (Fig. 3, C and D and fig. S4B and table S3). Enrichment of CD80 on *C9orf72*$^{-/-}$ microglia, an outcome not observed in *C9orf72*$^{+/-}$ mice, modeled the phenotype in human ALS spinal cord.

C9ORF72 restrains CD80 trafficking in response to inflammatory stimuli.

Protein abundance on the cell surface depends, in part, on the dynamic balance between externalization and internalization of vesicles. To glean additional insight into regulation of co-stimulation by *C9orf72*, we first tested whether *C9orf72* LOF affected receptor-mediated endocytosis of CD80 or the lipopolysaccharide (LPS) sensor toll-like receptor 4 (TLR4). Splenic macrophages from *C9orf72*$^{-/-}$ mice showed no deficit in CD80 or TLR4 internalization relative to *C9orf72*$^{+/+}$ cells (fig. S5, A and B). Next, we used CRISPR/Cas9 to edit *C9orf72* in Raw 264.7 mouse macrophages (*C9orf72*$^{\Delta}$) and compared these cells with unedited isogenic controls (*C9orf72*^{WT}). We found that CD80 accumulated to a greater

extent on the surface of *C9orf72*$^{\Delta}$ cells than *C9orf72*^{WT} cells in response to the TLR2 agonist Pam_3csk_4 or the TLR7/8 agonist R848, but CD80 was not elevated to a greater extent in response to LPS or the TLR3 agonist poly(I:C) (Fig. 4A and fig. S5, C and D). MHCII surface accumulation was not potentiated by *C9orf72* deficiency (Fig. 4A and fig. S5, C and D). The differential responsiveness to TLR-dependent stimuli may explain why *C9orf72*$^{-/-}$ macrophages accumulate CD80, but not MHCII, on their cell surface (Fig. 2E).

Following exposure to Pam_3csk_4, CD80 was enriched in whole cell lysate of *C9orf72*$^{\Delta}$ cells relative to *C9orf72*^{WT} controls (Fig. 4B) and immunostaining revealed that CD80 accumulated on the perimeter of stimulated *C9orf72*$^{\Delta}$ cells (Fig. 4C). Given that C9ORF72 can act as a GAP for small GTPases involved in actin cytoskeleton and vesicle movement (6–8), we hypothesized the altered abundance of CD80 in *C9orf72*$^{\Delta}$ cells was due to aberrant vesicle trafficking. To test this, we added Apilimod, an inhibitor of the lipid kinase enzyme PIKfyve that regulates endomembrane homeostasis (9), to cells 3 hours after Pam_3csk_4, when most changes in TLR signaling and CD80 expression had already occurred. We then measured CD80 by flow cytometry (Fig. 4D). Apilimod treatment caused CD80 to accumulate inside *C9orf72*$^{\Delta}$ cells rather than on their surface (Fig. 4, E and F), suggesting that CD80 traffics through PIKfyve-dependent vesicles in myeloid cells.

Next, we considered whether inflammatory cytokines enriched in *C9orf72*$^{-/-}$ plasma could elicit aberrant co-stimulation. Recombinant interferon (IFN)-γ exposure caused *C9orf72*$^{\Delta}$ mouse macrophages, but not *C9orf72*^{WT} cells, to accumulate CD80 in total lysate and on the surface (Fig. 4, G and H). Whereas recombinant IL-17A (rIL-17A) alone did not affect expression of CD80, co-administration of rIL-17A with IFN-γ further enhanced CD80 in a *C9orf72*-dependent manner (Fig. 4, G and H). Moreover, introduction of a human *C9ORF72*-expressing plasmid prior to cytokine stimulation reduced CD80 induction on *C9orf72*$^{\Delta}$ cells (Fig. 4I). Together these findings suggest that C9ORF72 restrains CD80 trafficking to the cell surface in response to microbial-derived agonists of TLR2, TLR7, and TLR8 as well as IL-17A and IFN-γ, cytokines produced by pathogenic Th17 cells.

Induction of lysosomal exocytosis by the lysotrophic agent chloroquine was impaired in *C9orf72*$^{\Delta}$ cells relative to *C9orf72*^{WT} cells, as illustrated by the reduced abundance of Lamp1 on the cell surface (fig. S5E). The muted response of *C9orf72*$^{\Delta}$ cells to chloroquine correlated with elevation of lysosomal pH (fig. S5F) and is consistent with reduced protonation of chloroquine that leads to its entrapment in the organelle (46). After TLR2 stimulation, *C9orf72*$^{\Delta}$ cells were more likely to adopt a CD80^{hi} Lamp1^{lo} phenotype, rather than a CD80^{lo} Lamp1^{hi} phenotype (fig. S5, G and H). This raised the possibility that *C9orf72* governs the transition to unique myeloid cell states. In support, we found that CD80^{hi} Lamp1^{lo} and CD80^{lo} Lamp1^{hi} splenic macrophages were elevated in *C9orf72*$^{-/-}$ mice and *C9orf72*$^{2Lox/2Lox}$;*LysM*-Cre+ mice compared with age matched controls (fig. S5, I and J). Future efforts will delineate how these divergent macrophage populations contribute to organismal health and disease.

Microglia and endothelial cells participate in *C9orf72* LOF-dependent neuroinflammation.

C9orf72$^{-/-}$ mice develop neuroinflammatory features that resemble *C9ORF72*-ALS/FTD (10, 11, 27, 28). To explore the temporal and anatomic basis of these phenotypes, we

performed single-cell RNA sequencing of the dissociated cortex and lumbar spinal cord from *C9orf72*$^{+/+}$ and *C9orf72*$^{-/-}$ littermates at 2, 4, and 8 months of age (Fig. 5A). Quality control yielded 50,578 sequenced cells for downstream analysis. We used Seurat (47) to separate cells into clusters with t-stochastic neighbor embedding (tSNE) dimensionality reduction and identified microglia (complement C1q subunit A (*C1qa*)), endothelial cells (claudin-5 (*Cldn5*), vascular endothelial growth factor receptor 1 (*Flt1*)), astrocytes (connexin 43 (*Gja1*)), pericytes (proteolipid protein 1 (*Plp1*)), oligodendrocytes (cyclic nucleotide phosphodiesterase (*Cnp*)), and neurons (doublecourtin (*Dcx*), synaptosomal-associated protein 25 (*Snap25*), stathmin 2 (*Stmn2*)) from each library (fig. S6, A to D) and found the proportion of each cell type consistent across time points, tissues, and genotypes (fig. S6E).

The greatest number of significant differentially expressed genes (DEGs, $p < 0.05$) occurred between *C9orf72*$^{+/+}$ and *C9orf72*$^{-/-}$ endothelial cells (236 spinal cord DEGs; 264 cortex DEGs), followed by microglia (145 spinal cord DEGs; 202 cortex DEGs), astrocytes (90 spinal cord DEGs; 110 cortex DEGs), pericytes (25 spinal cord DEGs; 45 cortex DEGs) and oligodendrocytes (39 spinal cord DEGs; 0 cortex DEGs) (Fig. 5B and data file S1). Relatively few neurons were sequenced after myelin removal, so these cells were excluded from the DEG analysis. To determine whether *C9orf72* regulates a shared set of genes in distinct cell types of the brain, we generated a z-score of all DEGs elevated in each cell population and compared the expression of this module across cellular populations in the dataset. Genes that were upregulated in *C9orf72*$^{-/-}$ endothelial cells showed elevated expression in microglia and pericytes (Fig. 5C). Reciprocally, genes upregulated in *C9orf72*$^{-/-}$ microglia were modestly upregulated in endothelial cells (Fig. 5D). In contrast, genes upregulated in *C9orf72*$^{-/-}$ astrocytes were expressed to a similar extent across the other cell populations profiled (Fig. 5E).

Gene ontology (GO) analysis of DEGs in each population demonstrated that *C9orf72*$^{-/-}$ microglia and endothelial cells displayed concordant changes in pathways of immune system processes, such as antigen processing and presentation, defense response to other organisms, and response to viruses (Fig. 5, F and G and fig. S6, F and G). Pathways elevated in *C9orf72*$^{-/-}$ astrocytes related to peptide metabolism, glycolysis, and myelin sheath (fig. S6H). We note that *C9orf72*$^{-/-}$ microglia, endothelial cells, and astrocytes all exhibited downregulation of genes involved in oxidative phosphorylation (*mt-Atp6*, *mt-Co1*, *mt-Co3*) (Fig. 5, H to K and fig. S6, I and J), consistent with a previously reported role for C9ORF72 in regulation of the electron transport chain (48). At 2 months of age, *C9orf72*$^{-/-}$ microglia and endothelial cells displayed significant elevation of MHCI genes (*H2-D1*, *H2-T23, H2-K1*), whereas at 8 months of age we found a shared elevation of interferon-inducible genes (*Ifi27l2a*, *Ifitm3, Slfn2*) ($p < 0.05$) (Fig. 5, J and K). At 4 months of age, *C9orf72*$^{-/-}$ microglia expressed chemokines (*Ccl2*, *Ccl3*, *Ccl4*) and cytokines (*Il-1b*, *Il-1a*, *Tnf*) that attract and activate peripheral immune cells (Fig. 5J), whereas *C9orf72*$^{-/-}$ endothelial cells expressed genes associated with circulatory system development (*Tfrc, Sox18*, *Ankrd37*) (Fig. 5K).

Lall and colleagues (49) performed single cell transcriptomics of cortex from *C9orf72*$^{-/-}$ mice and identified an interferon response microglia (IRM) and activated response microglia

(ARM) gene signature at 17 months of age in *C9orf72*$^{-/-}$ animals. We found 13 IRM genes and 33 ARM genes to be differentially expressed in *C9orf72*$^{-/-}$ microglia from our study (fig. S7, A and B). Microglial pathways shared between the studies included viral process, defense response to other organisms, and response to type II interferon (fig. S7C). Elevation of the IRM gene module in our study was greatest in *C9orf72*$^{-/-}$ microglia at 8 months of age (fig. S7, D and E). Comparison of endothelial cells between the studies revealed 53 concordant upregulated DEGs and 12 shared downregulated DEGs (fig. S7, F and G) and shared pathways included antigen processing and presentation, defense response to other organisms, and response to type II interferon (fig. S7H).

To determine whether the changes in gene expression we observed in the CNS were conserved in peripheral immune cells, we performed single cell RNA sequencing of *C9orf72*$^{-/-}$ and *C9orf72*$^{+/+}$ splenocytes and identified macrophages (*Lyz2*), conventional DCs (*Itgax*), plasmacytoid DCs (*Siglec-H*), neutrophils (*Ly6G*), T cells (*Cd3e, Cd4, Cd8a*), B cells (*Cd19*), plasma cells (*Sdc1*) and red blood cells (*Hba-a1*) (fig. S8, A and B). *C9orf72*$^{-/-}$ myeloid and lymphoid cell populations exhibited concordant changes in genes associated with ALS, regulation of organelle organization, and antigen processing and presentation that mirrored alterations in microglia (fig. S8, C to F). We validated that Apolipoprotein E (*Apoe*) and Cathepsin B (*Ctsb*) are elevated in *C9orf72*$^{-/-}$ macrophages (fig. S8, G and H and table S4). These data suggest that *C9orf72* regulates overlapping gene programs in the CNS and the periphery, potentially in response to inflammatory cues.

IL-17A promotes *C9orf72*$^{-/-}$ dependent systemic inflammation and CD80 co-stimulation.

We hypothesized that IL-17A is an important mediator of inflammation in *C9orf72*$^{-/-}$ mice because transplantation of *C9orf72*$^{-/-}$ bone marrow into *C9orf72*$^{+/+}$ mice caused IL-17A accumulation and fatal autoinflammatory disease (11), whereas treatment of *C9orf72*$^{-/-}$ mice with antibiotics or fecal microbial transplantation reduced IL-17A abundance and ameliorated autoimmune and inflammatory phenotypes (27). To test this hypothesis, we generated and intercrossed *C9orf72*$^{+/-}$ *Il-17a*$^{+/-}$ mice from different breeding pairs to make littermates for study (fig. S9A). We observed no overt inflammation in *C9orf72*$^{+/+}$ mice independent of the copies of *Il-17a* (fig. S9, B to F), so these animals were pooled (*C9orf72*$^{+/+}$*;Il-17a*^{all}) for comparisons. Relative to *C9orf72*$^{+/+}$*;Il-17a*^{all} controls, *C9orf72*$^{-/-}$*;Il-17a*$^{+/+}$ mice developed features of systemic inflammation that included neutrophilia (fig S9B), reduced platelet count (fig. S9C), splenomegaly (Fig. 6A, fig. S9D), and mLN hyperplasia (Fig. 6B, fig. S9E). In contrast, homozygous deletion of *Il-17a* in *C9orf72*$^{-/-}$ mice alleviated lymphocytosis and neutrophilia in spleens and mLNs (Fig. 6, A and B). Th17 cells and T_{reg} cells were reduced in *C9orf72*$^{-/-}$*;Il-17a*$^{-/-}$ mLNs but not spleens relative to *C9orf72*$^{-/-}$;*Il-17a*$^{+/+}$ mice (fig. S9, G to J). Moreover, *Il-17a* deficiency prevented the accumulation of *C9orf72*$^{-/-}$ CD80^{hi} myeloid cells in mLN and spinal cord (Fig. 6, C to E and fig. S9K) and reduced IgM but not IgG autoantibodies in *C9orf72*$^{-/-}$ plasma (fig S10A and B). Thus, these data suggest that in the absence of C9ORF72, IL-17A augments CD80 co-stimulation in the gut and CNS.

IL-17A neutralization improves motor function and neuronal health in *C9orf72*$^{-/-}$ mice.

Lastly, we investigated whether IL-17A neutralization could reverse established neuroinflammation in *C9orf72*$^{-/-}$ mice. We aged an additional cohort of *C9orf72*$^{+/+}$ (n=38; 22 female:16 male) and *C9orf72*$^{-/-}$ mice (n=36; 11 female:25 male) and distributed mutants into treatment groups based on rotarod performance and blood measurements (fig. S11, A to D). Then we began treatment with vehicle (*C9orf72*$^{+/+}$ vehicle, n=22 female, n=16 male), isotype control antibody (*C9orf72*$^{-/-}$ isotype, n=6 female, n=12 male) or anti-IL-17A neutralizing antibody (*C9orf72*$^{-/-}$ anti-IL-17A, n=5 female, n=13 male), followed by analysis of peripheral organ and brain inflammation after 6 weeks (Fig. 7A). We found that improvement of motor function over the study duration was significantly greater in *C9orf72*$^{-/-}$ anti-IL-17A females (Fig. 7B; p = 0.0022, one-way ANOVA with Tukey's correction for multiple comparisons) and males (Fig. 7C; p = 0.0343, one-way ANOVA with Tukey's correction for multiple comparisons) relative to *C9orf72*$^{+/+}$ vehicle controls. In contrast, no difference in motor improvement was observed between *C9orf72*$^{+/+}$ vehicle and *C9orf72* $^{-/-}$ isotype mice (Fig. 7, B and C). Circulating neutrophils were reduced in female, but not male, *C9orf72*$^{-/-}$ anti-IL-17A mice relative to *C9orf72*$^{-/-}$ isotype controls (Fig. 7, D and E) although other measures of peripheral inflammation did not differ between *C9orf72*$^{-/-}$ anti-IL-17A and *C9orf72*$^{-/-}$ isotype groups (fig. S11, E to J). Moreover, no deaths occurred in the *C9orf72* $^{+/+}$ vehicle group; however, two *C9orf72*$^{-/-}$ isotype males and two *C9orf72*$^{-/-}$ anti-IL-17A females died over the treatment course (fig. S11, K to M). Finally, spinal cord cells from male and female *C9orf72*$^{-/-}$ isotype mice displayed elevated expression of *Apoe*, Histocompatibility 2-Q7 region (*H2-Q7*), Interferon induced transmembrane protein 3 (*Ifitm3*), and Interleukin 1 beta (*Il1b)*; in contrast, this neuroinflammatory gene signature was not different between *C9orf72*$^{-/-}$ anti-IL-17A cells relative to *C9orf72*$^{+/+}$ vehicle controls and *Apoe* was lower in *C9orf72*$^{-/-}$ anti-IL-17A compared with *C9orf72*$^{-/-}$ isotype (Fig.7F).

DISCUSSION

This work sought to address two interrelated questions: To what extent are the immune phenotypes observed in *C9orf72*-deficient mice attributable to the function of this gene in hematopoietic cells and through what mechanism does C9ORF72 promote organismal health? Here we report that *C9orf72* acts within the myeloid lineage, particularly in macrophages and monocytes, to prevent the initiation of autoimmune disease. Our findings support a model in which C9ORF72 normally restrains CD80 surface expression within myeloid cells following exposure to inflammatory stimuli. However, when functional *C9orf72* expression declines, CD80 is aberrantly trafficked to the cell surface, where it provides an antigen-independent co-stimulatory signal that promotes activation of T cells, including those with reactivity to self-antigens. Over time, this chronic co-stimulation leads to broad loss of tolerance and premature mortality. In addition, our findings revealed a complementary role for *C9orf72* to limit IL-17A-dependent inflammation. Specifically, IL-17A acts in a feed-forward manner to enhance myeloid CD80 co-stimulation in the spinal cord and draining lymph nodes of the gut, where it enables T helper cell differentiation.

The IL-17A inflammatory axis may be a convergent pathologic mechanism across diverse forms of ALS/FTD. As a biomarker, IL-17A is enriched in the serum and spinal fluid of patients with ALS/FTD, including those with a *C9ORF72* mutation (23–26). In addition, Th17 cells are present at a higher frequency in the blood of patients with ALS at disease onset and correlate with a faster rate of progression (21, 50, 51). IL-17A may act directly to induce neural degeneration (52, 53), or indirectly by disruption of brain vasculature (54) or the promotion of neurotoxic cells such as neutrophils (55). Indeed, neutrophils are enriched in the blood and cerebral spinal fluid of patients with sporadic ALS and neutrophilia negatively correlates with rate of survival (56, 57). Our demonstration that *C9ORF72* ALS microglia increase expression of CD80, that IL-17A and IFN-γ induce CD80 expression, and that depletion of *Il-17a* attenuates CD80 in the spinal cord of *C9orf72*-deficient mice further elaborate how IL-17A and aberrant co-stimulation (58) might exacerbate motor neuron disease. Encouragingly for patients, therapies that target IL-17A are approved by the United States Food and Drug Administration (59) and could be quickly repurposed to treat ALS/FTD.

In addition to governing IL-17A production, we found that *C9orf72*-LOF associated with altered B cell immunoglobulin class switching. The transition from IgM to IgG is important for anti-viral and anti-cancer immunity, in part due to an increase in the affinity of the antibodies for antigen as well as enhanced $F_c\gamma$ receptor IIIa-mediated cytotoxicity (60). The regulation of class switch recombination is complex and involves B cell-intrinsic signals and extrinsic signals such as cytokines provided by APC-dependent helper T cells. Similarly, the decision of naïve T cells to differentiate into T helper type 1, Th17 or T_{reg} cells or to trans-differentiate during chronic immune responses (61) is dependent on the strength of T cell receptor signaling as well as the local milieu of cytokines and ligands present (62, 63). Future efforts will focus on molecular regulation of B cell class switch recombination and T cell fate determination by C9ORF72.

Bulk RNA sequencing of brain samples from patients with *C9ORF72* ALS has demonstrated an enrichment of genes related to antigen processing and presentation and anti-viral immunity (28, 64). Our finding that microglia from *C9orf72*-deficient mice express a similar signature is consistent with previous studies that have profiled the nervous system of these mutant mice using bulk and single cell RNA sequencing (10, 49). By extending our single cell analysis to other glial populations, we discovered concordantly enriched gene programs in *C9orf72*-deficient endothelial cells. This convergence may have occurred, in part, as a response to ongoing systemic inflammation and disruption of the blood spinal cord barrier (27) as evidenced by increased titers of autoantibodies against Aquaporin 4, as well as evidence of increased activation of the coagulation and complement cascades. Since endothelial cells share a common developmental origin with *Vav1*+ hematopoietic stem cells (31), induce *Mx1* in response to interferon (32), and express STING (28, 65), our findings raise the possibility that *C9orf72* may act within the brain vasculature to promote tolerance to neural antigens. An important future experiment will be to determine whether rescuing *C9ORF72* expression in the neurovascular unit can improve blood spinal cord barrier integrity that becomes disrupted in patients with ALS (66, 67).

Our study is not without limitations. Although we measured CD80 expression in spinal cord from four patients with *C9ORF72* ALS and three non-ALS controls, a larger survey of sporadic and familial ALS and FTD patients will help to determine whether microglia CD80 is a general feature of the disease or a specific consequence of the *C9ORF72* mutation. To elucidate the relationship between CD80 co-stimulation, motor neuron loss, and rate of motor decline, evaluation of CD80 across affected and unaffected brain regions of patients annotated for fast or slow disease progression should be performed. Whereas IL-17A neutralization improved motor function and suppressed neuroinflammation in aged *C9orf72*$^{-/-}$ mice, this therapy was not sufficient to reduce spleen weight or increase platelet counts. Prophylactic neutralization of IL-17A at a younger age may be required to prevent or reverse systemic inflammation and autoimmunity in this model. Moreover, by following the natural history of hundreds of mutant mice, we found that *C9orf72*$^{-/-}$ males tended to die at younger ages than *C9orf72*$^{-/-}$ females. A male predominance is also observed in ALS but this sex-bias is incompletely understood (68). Our observation that IL-17A neutralization suppressed circulating neutrophils in female, but not male, *C9orf72*$^{-/-}$ mice may support a role for estrogen or X-linked genes in the regulation of IL-17-mediated granulopoiesis. In conclusion, our study has identified an important role for *C9orf72* in myeloid and lymphoid cells to oppose autoimmunity and implicates IL-17A as a key effector of neuroinflammation in *C9orf72*-deficient mice. The role of *C9ORF72* haploinsufficiency in ALS/FTD is still unclear and is likely to act in conjunction with environmental exposures (16, 27, 69), other ALS and FTD risk alleles (70), and GOF effects of the *C9ORF72* mutation. Ultimately, a cure for ALS and FTD may involve a combination of approaches such as correction of the causal gene mutation, augmentation of protein and metabolic homeostasis, and reorientation of the immune system to promote neural protection and tissue regeneration. IL-17A neutralization may be one such complementary approach for ALS and FTD.

MATERIALS AND METHODS

Study design

The goal of this study was to identify cell types and pathways that contribute to autoimmunity and inflammation in *C9orf72* LOF mice. The experimental design involved age-matched evaluation of *C9orf72* mutant and control mice paired with mass cytometry, flow cytometry, single cell sequencing, antibody-based therapeutic neutralization, and cellular and biofluidic analyses. Sample sizes were determined based on power calculations. Pre-defined euthanasia criteria and age for euthanasia was determined based on temporal characterization of systemic and neuroinflammation in this model. Neutrophil counts, platelet counts, and rotarod performance were used to assign mice into isotype antibody or anti-IL-17A antibody treatment groups so these disease measures did not differ between *C9or72*$^{-/-}$ mice prior to treatment. All subjects were coded so operators remained blinded to genotype during behavioral testing, tissue harvest, and outcome assessments. Numbers of mice and well replicates are indicated in figure legends.

Animals

All experimental protocols and procedures were approved by the Institutional Animal Care and Use Committees of Harvard University and Case Western Reserve University and were

in compliance with all relevant ethical regulations. Two independent cohorts of *C9orf72* LOF mice, initially developed and characterized at Harvard University Biological Research Infrastructure Building (HU BRI) (11, 27), were used this study. To establish a colony at Case Western Reserve University Wolstein Research Building (CWRU WRB), *C9orf72*$^{+/-}$ mice were backcrossed onto C57BL6/J for six generations at HU and were rederived by aseptic embryo transfer to generate founders for propagation. The fecal bacteria of mice at CWRU WRB more closely resembled mice reared in HU rather than C57BL6/J mice from Jackson Laboratory (10, 27) and *C9orf72*$^{-/-}$ developed inflammation and autoimmunity at CWRU WRB (fig. S12, A to E). Mice were housed with nestlet bedding on a 12-h light/dark cycle and provided ad libitum water and food (Prolab Isopro RMH 3000 (HU BRI) or Envigo Mouse/Rat Diet (CWRU WRB)). Embryo re-derivation was performed by collecting embryos from super-ovulated *C9orf72*$^{+/-}$ females, washing embryos, then surgical transfer using aseptic technique into the reproductive tract of pseudo-pregnant recipient females. The generation of *C9orf72* LOF animals with neomycin resistance cassette removed (neo deleted)was previously described (11). *C9orf72* conditional mice were obtained by material transfer agreement from Dr. Jeroen Pasterkamp (30). *Il-17a* knockout mice were a kind gift from Dr. Nicole Ward (71). Cre lines used in this study were obtained from Jackson labs and included *Vav1*-cre (31), *Mx1*-cre (32)), *Lyz2/LysM*-cre (33), *CD2*-cre (34), *CD19*-cre (35), *CD4*-cre (36) and *FoxP3*-cre (37). Tail DNA was lysed in Viagen digest buffer (102-T) supplemented with proteinase K (Roche) for 12 hours at 55°C. Genotyping PCR was performed using Amplitaq gold (Thermo) as outlined for each strain (fig. S1D).

Human tissue samples

Post-mortem frozen spinal cord sections from control individuals and *C9ORF72* carriers were obtained as previously described (78). This Health Insurance Portability and Accountability Act-compliant prospective study was approved by the Cleveland Clinic institutional review board and written informed consent was obtained from all participants. Eligibility required a diagnosis of ALS according to the revised El Escorial criteria.

Single cell sequencing

For dissociation of brain and spinal cord tissue for single cell sequencing, 2 mL glass pipette tips were used to homogenize the tissue and dissociated with papain (Worthington) supplemented with DNAse in Ca^{2+}-free serum-free Earle's Balanced Salt Solution pre-heated to 37°C. Tissue was dissociated at 37°C for 25-min, with homogenization after 10-mins using 1 mL plastic tip. After 25-min, the tissue was homogenized again with 1 mL plastic tip, filtered (70 μm), Dulbecco's Modified Eagle Medium (DMEM, Gibco) supplemented with 10% fetal bovine serum (FBS) added, then centrifuged at 300g for 10-min. Cells were subjected to myelin removal beads (Miltenyi), counted, diluted in Ca^{2+}-free HBSS with 0.5% Bovine Serum Albumin, and loaded into a Chromium Single Cell 3' Chip (10X Genomics) and processed following the manufacturer's instructions. Sequencing libraries were prepared with the Chromium Single Cell 3' library and Gel Bead kit v2 (10X Genomics). Libraries were sequenced on a Nova-seq 6000. Reads were aligned to the mouse genome assembly GRCm38. Count matrices were generated for each sample, and a combined UMI matrix was generated using merge. This matrix was first filtered for number of genes (nFeature) and percentage of mitochondrial and ribosomal genes (400<

nFeature_RNA < 4000, percent.mito < 25, percent.RPS < 15, percent.RPL < 15) and then normalized and scaled manually using default Seurat algorithm (v3.0.1) (47). After quality filtering, filtered barcodes were used to compute Shared nearest-neighbor graphs and *t*-SNE projections using the first 8 statistically significant Principal Components, then cell identity was assigned on broad cell type specific markers as previously described (72). Analysis of cellular subtypes were conducted by subsetting each cell type as separate group. Isolated barcodes were re-normalised and scaled and relevant PCs were used for re-clustering as a separate analysis. This newly scaled matrix was used for Differential Gene Expression analysis. gProfiler used to quantify KEGG and Gene ontology pathway enrichment of differentially expressed genes for each identified cluster. For spleens, Cell Ranger 2.2.0 used to process raw sequencing data to convert Illumina basecall files to fastq, aligned sequencing reads to mm10 transcriptome using STAR aligner (73) and quantified the expression of transcripts in each cell. Analysis of processed scRNAseq data in R using Seurat (74, 75) and tidyverse packages (76). K means clustering applied to assigned clusters using SPRING (77). Log fold enrichment of each gene within identified clusters mapped using Morpheus (https://software.broadinstitute.org/morpheus).

Macrophage and OTII T cell cocultures

Macrophages were isolated from single cell dissociated mLNs, spleens and colons using F4/80 positive selection beads (Miltenyi) as per the manufacturer's instructions. Macrophages were counted and plated in ventilated tubes in an incubator for 18 hours in T cell co-culture media containing RPMI 1640, 10% heat inactivated FBS (high grade Hyclone SH30084.03HI), 1% Sodium Pyruvate, 50 μM β-mercaptoethanol, 10 mM HEPES, 5 mL penicillin-streptomycin and Glutamax in the presence of 50 μg/mL $OVA_{323-339}$ peptide (Invivogen vac-isq). The following day, macrophages were centrifuged, washed in fresh media twice, and 5,000 cells per well were plated into 96 well round bottom tubes. $CD4^+$ $CD25^-$ OTII splenic T cells were bead enriched (Miltenyi), counted, and loaded with CFSE at 5 μg/mL for 20 mins in phosphate buffered saline (PBS); cells were then washed in complete medium, counted, diluted in T cell co-culture media supplemented with recombinant human IL-2 (Peprotech) (2.5 ng/mL), and plated at 40,000 cells per well onto the OVA-loaded macrophages. After 4 days in culture, cells were analyzed for CSFE dilution on a BD Fortessa.

IL-17A neutralization and motor behavior

Naïve animals were trained on the rotarod at constant speed of 4 RPM for 300 seconds at least one day before competitive assessment. For performance trials, the rotarod accelerated from 4 to 40 RPM over 300 seconds using Ugo Basile mouse RotaRod NG. Each trial day consisted of three tests per mouse, with each test separated by at least 20 minutes. Operator was blinded to animal genotype during trials. During the study period vehicle, anti-mouse IL-17A or IgG1 isotype control (InVivoMAb) was administered at a dose of 30 mg/kg intraperitoneally twice per week.

Statistical Analysis

A majority of the data was analyzed using Prism 10 (GraphPad Inc.). Unpaired t-test was used to test for significance between two groups. For distributions that did not meet the

assumption of normality using Kolmogorov-Smirnov test, we applied the Mann-Whitney U test. For comparisons across multiple conditions one- or two-way ANOVA was performed with Sidak's, Tukey's, or Dunnett's correction for multiple comparisons or Kruskal-Wallis test with Dunn's correction for multiple comparisons when data did not meet the assumption of normality using Kolmogorov-Smirnov test. Figure legends indicate each statistical test and n values that refer to the number of biological or well to well replicates. All cell culture experiments were repeated at least twice. Differences between groups were deemed significant at two-tailed $p < 0.05$. For comparison of surface antigen expression across spleen populations (CyTOF), a Bonferroni corrected T-test or Mann-Whitney test for non-normal distributions was performed to compare 2 groups: *C9orf72*$^{+/+}$ and *C9orf72*$^{-/-}$. The n=9 cell types of the spleen identified were treated as subgroups, so the Bonferroni correction was calculated as alpha divided by n or 0.05/9 = 0.0056. Single cell sequencing data were analyzed in R using the Seurat pipeline and genes expressed in >25% of cells with Log_2 Fold change >0.25 adjusted p-values <0.05 were considered significant. Survival data were assessed by Gehan-Breslow-Wilcoxon test.

Supplementary Material

Refer to Web version on PubMed Central for supplementary material.

Acknowledgments:

We thank Eric Haas and the DFCI Mass Cytometry core for assistance with sample acquisition, Kayleigh Rutherford, Shannan Ho Sui, and John Hutchinson of the Harvard Chan Bioinformatics core for support with spleen single cell RNA sequencing, and the UTSW Microarray Core Facility for aid with autoantigen microarrays. We thank Bruce D. Trapp for kindly providing human spinal cord sections. *Il-17a* knockout mice were a kind gift from Dr. Nicole Ward (71).

Funding:

Funding for these studies was provided by The Merkin Fund at Broad Institute (to K.E.), Target ALS grant (to K.E.), UCB Biopharma SRL grant (to K.E. & I.K.), National Institute of Health grants: National Institute of Neurological Disorders and Stroke 5R01NS089742 (to K.E.) and 5R35NS097303-06 (to Cleveland Clinic Lerner Research Institute); National Institute of Aging 5K99AG057808-02 and 4R00AG057808-03 (to AB), and NIH Office of the Director S10-NIH OD021559 (to Case Comprehensive Cancer Center Cytometry & Microscopy Shared Resource Center).

Data and materials availability:

All data associated with this study are in the paper or the supplementary materials. RNA sequencing datasets can be assessed through GEO accession #s GSE252888. *C9orf72*^{2Lox} mice were obtained from Dr. Jeroen Pasterkamp through material transfer agreement.

REFERENCES

1. Majounie E, Renton AE, Mok K, Dopper EGP, Waite A, Rollinson S, Chiò A, Restagno G, Nicolaou N, Simon-Sanchez J, van Swieten JC, Abramzon Y, Johnson JO, Sendtner M, Pamphlett R, Orrell RW, Mead S, Sidle KC, Houlden H, Rohrer JD, Morrison KE, Pall H, Talbot K, Ansorge O, Chromosome 9-ALS/FTD Consortium, French research network on FTLD/FTLD/ALS, ITALSGEN Consortium, Hernandez DG, Arepalli S, Sabatelli M, Mora G, Corbo M, Giannini F, Calvo A, Englund E, Borghero G, Floris GL, Remes AM, Laaksovirta H, McCluskey L, Trojanowski JQ, Van Deerlin VM, Schellenberg GD, Nalls MA, Drory VE, Lu C-S, Yeh T-H, Ishiura H, Takahashi Y, Tsuji S, Le Ber I, Brice A, Drepper C, Williams N, Kirby J, Shaw P, Hardy J, Tienari PJ,

Heutink P, Morris HR, Pickering-Brown S, Traynor BJ, Frequency of the C9orf72 hexanucleotide repeat expansion in patients with amyotrophic lateral sclerosis and frontotemporal dementia: a cross-sectional study. Lancet Neurol 11, 323–330 (2012). [PubMed: 22406228]

2. Donnelly CJ, Zhang P-W, Pham JT, Haeusler AR, Heusler AR, Mistry NA, Vidensky S, Daley EL, Poth EM, Hoover B, Fines DM, Maragakis N, Tienari PJ, Petrucelli L, Traynor BJ, Wang J, Rigo F, Bennett CF, Blackshaw S, Sattler R, Rothstein JD, RNA toxicity from the ALS/FTD C9ORF72 expansion is mitigated by antisense intervention. Neuron 80, 415–428 (2013). [PubMed: 24139042]
3. Ash PEA, Bieniek KF, Gendron TF, Caulfield T, Lin W-L, Dejesus-Hernandez M, van Blitterswijk MM, Jansen-West K, Paul JW, Rademakers R, Boylan KB, Dickson DW, Petrucelli L, Unconventional translation of C9ORF72 GGGGCC expansion generates insoluble polypeptides specific to c9FTD/ALS. Neuron 77, 639–646 (2013). [PubMed: 23415312]
4. Mori K, Weng S-M, Arzberger T, May S, Rentzsch K, Kremmer E, Schmid B, Kretzschmar HA, Cruts M, Van Broeckhoven C, Haass C, Edbauer D, The C9orf72 GGGGCC repeat is translated into aggregating dipeptide-repeat proteins in FTLD/ALS. Science 339, 1335–1338 (2013). [PubMed: 23393093]
5. Belzil VV, Bauer PO, Prudencio M, Gendron TF, Stetler CT, Yan IK, Pregent L, Daughrity L, Baker MC, Rademakers R, Boylan K, Patel TC, Dickson DW, Petrucelli L, Reduced C9orf72 gene expression in c9FTD/ALS is caused by histone trimethylation, an epigenetic event detectable in blood. Acta Neuropathol 126, 895–905 (2013). [PubMed: 24166615]
6. Tang D, Sheng J, Xu L, Zhan X, Liu J, Jiang H, Shu X, Liu X, Zhang T, Jiang L, Zhou C, Li W, Cheng W, Li Z, Wang K, Lu K, Yan C, Qi S, Cryo-EM structure of C9ORF72–SMCR8–WDR41 reveals the role as a GAP for Rab8a and Rab11a. Proc Natl Acad Sci USA 117, 9876–9883 (2020). [PubMed: 32303654]
7. Su M-Y, Fromm SA, Zoncu R, Hurley JH, Structure of the C9orf72 ARF GAP complex that is haploinsufficient in ALS and FTD. Nature 585, 251–255 (2020). [PubMed: 32848248]
8. Sivadasan R, Hornburg D, Drepper C, Frank N, Jablonka S, Hansel A, Lojewski X, Sterneckert J, Hermann A, Shaw PJ, Ince PG, Mann M, Meissner F, Sendtner M, C9ORF72 interaction with cofilin modulates actin dynamics in motor neurons. Nat Neurosci 19, 1610–1618 (2016). [PubMed: 27723745]
9. Shi Y, Lin S, Staats KA, Li Y, Chang W-H, Hung S-T, Hendricks E, Linares GR, Wang Y, Son EY, Wen X, Kisler K, Wilkinson B, Menendez L, Sugawara T, Woolwine P, Huang M, Cowan MJ, Ge B, Koutsodendris N, Sandor KP, Komberg J, Vangoor VR, Senthilkumar K, Hennes V, Seah C, Nelson AR, Cheng T-Y, Lee S-JJ, August PR, Chen JA, Wisniewski N, Hanson-Smith V, Belgard TG, Zhang A, Coba M, Grunseich C, Ward ME, van den Berg LH, Pasterkamp RJ, Trotti D, Zlokovic BV, Ichida JK, Haploinsufficiency leads to neurodegeneration in C9ORF72 ALS/FTD human induced motor neurons. Nat Med 24, 313–325 (2018). [PubMed: 29400714]
10. O'Rourke JG, Bogdanik L, Yáñez A, Lall D, Wolf AJ, Muhammad AKMG, Ho R, Carmona S, Vit JP, Zarrow J, Kim KJ, Bell S, Harms MB, Miller TM, Dangler CA, Underhill DM, Goodridge HS, Lutz CM, Baloh RH, C9orf72 is required for proper macrophage and microglial function in mice. Science 351, 1324–1329 (2016). [PubMed: 26989253]
11. Burberry A, Suzuki N, Wang J-Y, Moccia R, Mordes DA, Stewart MH, Suzuki-Uematsu S, Ghosh S, Singh A, Merkle FT, Koszka K, Li Q-Z, Zon L, Rossi DJ, Trowbridge JJ, Notarangelo LD, Eggan K, Loss-of-function mutations in the C9ORF72 mouse ortholog cause fatal autoimmune disease. Sci Transl Med 8, 347ra93 (2016).
12. Jiang J, Zhu Q, Gendron TF, Saberi S, McAlonis-Downes M, Seelman A, Stauffer JE, Jafar-Nejad P, Drenner K, Schulte D, Chun S, Sun S, Ling S-C, Myers B, Engelhardt J, Katz M, Baughn M, Platoshyn O, Marsala M, Watt A, Heyser CJ, Ard MC, De Muynck L, Daughrity LM, Swing DA, Tessarollo L, Jung CJ, Delpoux A, Utzschneider DT, Hedrick SM, de Jong PJ, Edbauer D, Van Damme P, Petrucelli L, Shaw CE, Bennett CF, Da Cruz S, Ravits J, Rigo F, Cleveland DW, Lagier-Tourenne C, Gain of Toxicity from ALS/FTD-Linked Repeat Expansions in C9ORF72 Is Alleviated by Antisense Oligonucleotides Targeting GGGGCC-Containing RNAs. Neuron 90, 535–550 (2016). [PubMed: 27112497]
13. Atanasio A, Decman V, White D, Ramos M, Ikiz B, Lee H-C, Siao C-J, Brydges S, LaRosa E, Bai Y, Fury W, Burfeind P, Zamfirova R, Warshaw G, Orengo J, Oyejide A, Fralish M, Auerbach W, Poueymirou W, Freudenberg J, Gong G, Zambrowicz B, Valenzuela D, Yancopoulos G,

Murphy A, Thurston G, Lai K-MV, C9orf72 ablation causes immune dysregulation characterized by leukocyte expansion, autoantibody production, and glomerulonephropathy in mice. Sci Rep 6, 23204 (2016). [PubMed: 26979938]

14. Zhu Q, Jiang J, Gendron TF, McAlonis-Downes M, Jiang L, Taylor A, Diaz Garcia S, Ghosh Dastidar S, Rodriguez MJ, King P, Zhang Y, La Spada AR, Xu H, Petrucelli L, Ravits J, Da Cruz S, Lagier-Tourenne C, Cleveland DW, Reduced C9ORF72 function exacerbates gain of toxicity from ALS/FTD-causing repeat expansion in C9orf72. Nat Neurosci 23, 615–624 (2020). [PubMed: 32284607]
15. Ugolino J, Ji YJ, Conchina K, Chu J, Nirujogi RS, Pandey A, Brady NR, Hamacher-Brady A, Wang J, Loss of C9orf72 Enhances Autophagic Activity via Deregulated mTOR and TFEB Signaling. PLOS Genetics 12, e1006443 (2016). [PubMed: 27875531]
16. Chiò A, Mazzini L, D'Alfonso S, Corrado L, Canosa A, Moglia C, Manera U, Bersano E, Brunetti M, Barberis M, Veldink JH, van den Berg LH, Pearce N, Sproviero W, McLaughlin R, Vajda A, Hardiman O, Rooney J, Mora G, Calvo A, Al-Chalabi A, The multistep hypothesis of ALS revisited. Neurology 91, e635–e642 (2018). [PubMed: 30045958]
17. Turner MR, Goldacre R, Ramagopalan S, Talbot K, Goldacre MJ, Autoimmune disease preceding amyotrophic lateral sclerosis. Neurology 81, 1222–1225 (2013). [PubMed: 23946298]
18. Miller ZA, Sturm VE, Camsari GB, Karydas A, Yokoyama JS, Grinberg LT, Boxer AL, Rosen HJ, Rankin KP, Gorno-Tempini ML, Coppola G, Geschwind DH, Rademakers R, Seeley WW, Graff-Radford NR, Miller BL, Increased prevalence of autoimmune disease within C9 and FTD/MND cohorts. Neurol Neuroimmunol Neuroinflamm 3, e301 (2016). [PubMed: 27844039]
19. Turner MR, Cagnin A, Turkheimer FE, Miller CCJ, Shaw CE, Brooks DJ, Leigh PN, Banati RB, Evidence of widespread cerebral microglial activation in amyotrophic lateral sclerosis: an [11C] (R)-PK11195 positron emission tomography study. Neurobiol Dis 15, 601–609 (2004). [PubMed: 15056468]
20. Zürcher NR, Loggia ML, Lawson R, Chonde DB, Izquierdo-Garcia D, Yasek JE, Akeju O, Catana C, Rosen BR, Cudkowicz ME, Hooker JM, Atassi N, Increased in vivo glial activation in patients with amyotrophic lateral sclerosis: Assessed with [11C]-PBR28. Neuroimage Clin 7, 409–414 (2015). [PubMed: 25685708]
21. Jin M, Günther R, Akgün K, Hermann A, Ziemssen T, Peripheral proinflammatory Th1/Th17 immune cell shift is linked to disease severity in amyotrophic lateral sclerosis. Sci Rep 10, 5941 (2020). [PubMed: 32246039]
22. Mills KHG, IL-17 and IL-17-producing cells in protection versus pathology. Nat Rev Immunol 23, 38–54 (2023). [PubMed: 35790881]
23. Guo J, Yang X, Gao L, Zang D, Evaluating the levels of CSF and serum factors in ALS. Brain Behav 7, e00637 (2017). [PubMed: 28293476]
24. Fiala M, Chattopadhay M, La Cava A, Tse E, Liu G, Lourenco E, Eskin A, Liu PT, Magpantay L, Tse S, Mahanian M, Weitzman R, Tong J, Nguyen C, Cho T, Koo P, Sayre J, Martinez-Maza O, Rosenthal MJ, Wiedau-Pazos M, IL-17A is increased in the serum and in spinal cord CD8 and mast cells of ALS patients. J Neuroinflammation 7, 76 (2010). [PubMed: 21062492]
25. Pinilla G, Kumar A, Floaters MK, Pardo CA, Rothstein J, Ilieva H, Increased synthesis of pro-inflammatory cytokines in C9ORF72 patients. Amyotroph Lateral Scler Frontotemporal Degener , 1–11 (2021).
26. Hu WT, Chen-Plotkin A, Grossman M, Arnold SE, Clark CM, Shaw LM, McCluskey L, Elman L, Hurtig HI, Siderowf A, Lee VM-Y, Soares H, Trojanowski JQ, Novel CSF biomarkers for frontotemporal lobar degenerations. Neurology 75, 2079–2086 (2010). [PubMed: 21048198]
27. Burberry A, Wells MF, Limone F, Couto A, Smith KS, Keaney J, Gillet G, van Gastel N, Wang J-Y, Pietilainen O, Qian M, Eggan P, Cantrell C, Mok J, Kadiu I, Scadden DT, Eggan K, C9orf72 suppresses systemic and neural inflammation induced by gut bacteria. Nature 582, 89–94 (2020). [PubMed: 32483373]
28. McCauley ME, O'Rourke JG, Yáñez A, Markman JL, Ho R, Wang X, Chen S, Lall D, Jin M, Muhammad AKMG, Bell S, Landeros J, Valencia V, Harms M, Arditi M, Jefferies C, Baloh RH, C9orf72 in myeloid cells suppresses STING-induced inflammation. Nature 585, 96–101 (2020). [PubMed: 32814898]

29. Bagger FO, Kinalis S, Rapin N, BloodSpot: a database of healthy and malignant haematopoiesis updated with purified and single cell mRNA sequencing profiles. Nucleic Acids Research 47, D881–D885 (2019). [PubMed: 30395307]
30. Koppers M, Blokhuis AM, Westeneng H-J, Terpstra ML, Zundel CAC, Vieira de Sá R, Schellevis RD, Waite AJ, Blake DJ, Veldink JH, van den Berg LH, Pasterkamp RJ, C9orf72 ablation in mice does not cause motor neuron degeneration or motor deficits. Ann Neurol 78, 426–438 (2015). [PubMed: 26044557]
31. Georgiades P, Ogilvy S, Duval H, Licence DR, Charnock-Jones DS, Smith SK, Print CG, VavCre transgenic mice: a tool for mutagenesis in hematopoietic and endothelial lineages. Genesis 34, 251–256 (2002). [PubMed: 12434335]
32. Kühn R, Schwenk F, Aguet M, Rajewsky K, Inducible gene targeting in mice. Science 269, 1427–1429 (1995). [PubMed: 7660125]
33. Clausen BE, Burkhardt C, Reith W, Renkawitz R, Förster I, Conditional gene targeting in macrophages and granulocytes using LysMcre mice. Transgenic Res 8, 265–277 (1999). [PubMed: 10621974]
34. Siegemund S, Shepherd J, Xiao C, Sauer K, hCD2-iCre and Vav-iCre Mediated Gene Recombination Patterns in Murine Hematopoietic Cells. PLoS One 10, e0124661 (2015). [PubMed: 25884630]
35. Rickert RC, Rajewsky K, Roes J, Impairment of T-cell-dependent B-cell responses and B-l cell development in CD19-deficient mice. Nature 376, 352–355 (1995). [PubMed: 7543183]
36. Lee PP, Fitzpatrick DR, Beard C, Jessup HK, Lehar S, Makar KW, Pérez-Melgosa M, Sweetser MT, Schlissel MS, Nguyen S, Cherry SR, Tsai JH, Tucker SM, Weaver WM, Kelso A, Jaenisch R, Wilson CB, A critical role for Dnmt1 and DNA methylation in T cell development, function, and survival. Immunity 15, 763–774 (2001). [PubMed: 11728338]
37. Rubtsov YP, Rasmussen JP, Chi EY, Fontenot J, Castelli L, Ye X, Treuting P, Siewe L, Roers A, Henderson WR, Muller W, Rudensky AY, Regulatory T cell-derived interleukin-10 limits inflammation at environmental interfaces. Immunity 28, 546–558 (2008). [PubMed: 18387831]
38. Szychowski KA, Skóra B, Wójtowicz AK, Elastin-Derived Peptides in the Central Nervous System: Friend or Foe. Cell Mol Neurobiol 42, 2473–2487 (2022). [PubMed: 34374904]
39. Ayloo S, Lazo CG, Sun S, Zhang W, Cui B, Gu C, Pericyte-to-endothelial cell signaling via vitronectin-integrin regulates blood-CNS barrier. Neuron 110, 1641–1655.e6 (2022). [PubMed: 35294899]
40. Francesca B, Rezzani R, Aquaporin and Blood Brain Barrier. Curr Neuropharmacol 8, 92–96 (2010). [PubMed: 21119879]
41. Gomez-Arboledas A, Acharya MM, Tenner AJ, The Role of Complement in Synaptic Pruning and Neurodegeneration. Immunotargets Ther 10, 373–386 (2021). [PubMed: 34595138]
42. Crampton SP, Morawski PA, Bolland S, Linking susceptibility genes and pathogenesis mechanisms using mouse models of systemic lupus erythematosus. Disease Models & Mechanisms 7, 1033–1046 (2014). [PubMed: 25147296]
43. Allen E, Bakke AC, Purtzer MZ, Deodhar A, Neutrophil CD64 expression: distinguishing acute inflammatory autoimmune disease from systemic infections. Annals of the Rheumatic Diseases 61, 522–525 (2002). [PubMed: 12006325]
44. Zhao W, Beers DR, Hooten KG, Sieglaff DH, Zhang A, Kalyana-Sundaram S, Traini CM, Halsey WS, Hughes AM, Sathe GM, Livi GP, Fan G-H, Appel SH, Characterization of Gene Expression Phenotype in Amyotrophic Lateral Sclerosis Monocytes. JAMA Neurology 74, 677–685 (2017). [PubMed: 28437540]
45. Chen L, Flies DB, Molecular mechanisms of T cell co-stimulation and co-inhibition. Nat Rev Immunol 13, 227–242 (2013). [PubMed: 23470321]
46. Al-Bari Md. A. A., Chloroquine analogues in drug discovery: new directions of uses, mechanisms of actions and toxic manifestations from malaria to multifarious diseases. Journal of Antimicrobial Chemotherapy 70, 1608–1621 (2015). [PubMed: 25693996]
47. Stuart T, Butler A, Hoffman P, Hafemeister C, Papalexi E, Mauck WM, Hao Y, Stoeckius M, Smibert P, Satija R, Comprehensive Integration of Single-Cell Data. Cell 177, 1888–1902.e21 (2019). [PubMed: 31178118]

48. Wang T, Liu H, Itoh K, Oh S, Zhao L, Murata D, Sesaki H, Hartung T, Na CH, Wang J, C9orf72 regulates energy homeostasis by stabilizing mitochondrial complex I assembly. Cell Metab 33, 531–546.e9 (2021). [PubMed: 33545050]
49. Lall D, Lorenzini I, Mota TA, Bell S, Mahan TE, Ulrich JD, Davtyan H, Rexach JE, Muhammad AKMG, Shelest O, Landeros J, Vazquez M, Kim J, Ghaffari L, O'Rourke JG, Geschwind DH, Blurton-Jones M, Holtzman DM, Sattler R, Baloh RH, C9orf72 deficiency promotes microglial-mediated synaptic loss in aging and amyloid accumulation. Neuron 109, 2275–2291.e8 (2021). [PubMed: 34133945]
50. Mantovani S, Garbelli S, Pasini A, Alimonti D, Perotti C, Melazzini M, Bendotti C, Mora G, Immune system alterations in sporadic amyotrophic lateral sclerosis patients suggest an ongoing neuroinflammatory process. J Neuroimmunol 210, 73–79 (2009). [PubMed: 19307024]
51. Yazdani S, Seitz C, Cui C, Lovik A, Pan L, Piehl F, Pawitan Y, Kläppe U, Press R, Samuelsson K, Yin L, Vu TN, Joly A-L, Westerberg LS, Evertsson B, Ingre C, Andersson J, Fang F, T cell responses at diagnosis of amyotrophic lateral sclerosis predict disease progression. Nat Commun 13, 6733 (2022). [PubMed: 36347843]
52. Sommer A, Marxreiter F, Krach F, Fadler T, Grosch J, Maroni M, Graef D, Eberhardt E, Riemenschneider MJ, Yeo GW, Kohl Z, Xiang W, Gage FH, Winkler J, Prots I, Winner B, Th17 Lymphocytes Induce Neuronal Cell Death in a Human iPSC-Based Model of Parkinson's Disease. Cell Stem Cell 23, 123–131.e6 (2018). [PubMed: 29979986]
53. Jin M, Akgün K, Ziemssen T, Kipp M, Günther R, Hermann A, Interleukin-17 and Th17 Lymphocytes Directly Impair Motoneuron Survival of Wildtype and FUS-ALS Mutant Human iPSCs. International Journal of Molecular Sciences 22, 8042 (2021). [PubMed: 34360808]
54. Setiadi AF, Abbas AR, Jeet S, Wong K, Bischof A, Peng I, Lee J, Bremer M, Eggers EL, DeVoss J, Staton T, Herman A, von Büdingen H-C, Townsend MJ, IL-17A is associated with the breakdown of the blood-brain barrier in relapsing-remitting multiple sclerosis. J Neuroimmunol 332, 147–154 (2019). [PubMed: 31034962]
55. McGinley AM, Sutton CE, Edwards SC, Leane CM, DeCourcey J, Teijeiro A, Hamilton JA, Boon L, Djouder N, Mills KHG, Interleukin-17A Serves a Priming Role in Autoimmunity by Recruiting IL-1β-Producing Myeloid Cells that Promote Pathogenic T Cells. Immunity 52, 342–356.e6 (2020). [PubMed: 32023490]
56. Murdock BJ, Goutman SA, Boss J, Kim S, Feldman EL, Amyotrophic Lateral Sclerosis Survival Associates With Neutrophils in a Sex-specific Manner. Neurology - Neuroimmunology Neuroinflammation 8 (2021), doi:10.1212/NXI.0000000000000953.
57. Wei Q-Q, Hou Y-B, Zhang L-Y, Ou R-W, Cao B, Chen Y-P, Shang H-F, Neutrophil-to-lymphocyte ratio in sporadic amyotrophic lateral sclerosis. Neural Regen Res 17, 875–880 (2021).
58. Lincecum JM, Vieira FG, Wang MZ, Thompson K, De Zutter GS, Kidd J, Moreno A, Sanchez R, Carrion IJ, Levine BA, Al-Nakhala BM, Sullivan SM, Gill A, Perrin S, From transcriptome analysis to therapeutic anti-CD40L treatment in the SOD1 model of amyotrophic lateral sclerosis. Nat Genet 42, 392–399 (2010). [PubMed: 20348957]
59. Ceribelli A, Motta F, Vecellio M, Isailovic N, Ciccia F, Selmi C, Clinical Trials Supporting the Role of the IL-17/IL-23 Axis in Axial Spondyloarthritis. Frontiers in Immunology 12 (2021) (available at https://www.frontiersin.org/articles/10.3389/fimmu.2021.622770).
60. de Taeye SW, Bentlage AEH, Mebius MM, Meesters JI, Lissenberg-Thunnissen S, Falck D, Sénard T, Salehi N, Wuhrer M, Schuurman J, Labrijn AF, Rispens T, Vidarsson G, FcγR Binding and ADCC Activity of Human IgG Allotypes. Frontiers in Immunology 11 (2020) (available at https://www.frontiersin.org/articles/10.3389/fimmu.2020.00740).
61. Qiu R, Zhou L, Ma Y, Zhou L, Liang T, Shi L, Long J, Yuan D, Regulatory T Cell Plasticity and Stability and Autoimmune Diseases. Clinic Rev Allerg Immunol 58, 52–70 (2020).
62. Kleinewietfeld M, Hafler DA, The plasticity of human Treg and Th17 cells and its role in autoimmunity. Semin Immunol 25, 305–312 (2013). [PubMed: 24211039]
63. Bhattacharyya ND, Feng CG, Regulation of T Helper Cell Fate by TCR Signal Strength. Frontiers in Immunology 11 (2020) (available at https://www.frontiersin.org/articles/10.3389/fimmu.2020.00624).

64. Prudencio M, Belzil VV, Batra R, Ross CA, Gendron TF, Pregent LJ, Murray ME, Overstreet KK, Piazza-Johnston AE, Desaro P, Bieniek KF, DeTure M, Lee WC, Biendarra SM, Davis MD, Baker MC, Perkerson RB, van Blitterswijk M, Stetler CT, Rademakers R, Link CD, Dickson DW, Boylan KB, Li H, Petrucelli L, Distinct brain transcriptome profiles in C9orf72-associated and sporadic ALS. Nat Neurosci 18, 1175–1182 (2015). [PubMed: 26192745]

65. Anastasiou M, Newton GA, Kaur K, Carrillo-Salinas FJ, Smolgovsky SA, Bayer AL, Ilyukha V, Sharma S, Poltorak A, Luscinskas FW, Alcaide P, Endothelial STING controls T cell transmigration in an IFNI-dependent manner. JCI Insight 6, e149346.

66. Garbuzova-Davis S, Sanberg PR, Blood-CNS Barrier Impairment in ALS patients versus an animal model. Front Cell Neurosci 8, 21 (2014). [PubMed: 24550780]

67. Winkler EA, Sengillo JD, Sullivan JS, Henkel JS, Appel SH, Zlokovic BV, Blood–spinal cord barrier breakdown and pericyte reductions in amyotrophic lateral sclerosis. Acta Neuropathol 125, 111–120 (2013). [PubMed: 22941226]

68. Manjaly ZR, Scott KM, Abhinav K, Wijesekera L, Ganesalingam J, Goldstein LH, Janssen A, Dougherty A, Willey E, Stanton BR, Turner MR, Ampong M-A, Sakel M, Orrell RW, Howard R, Shaw CE, Leigh PN, Al-Chalabi A, The sex ratio in amyotrophic lateral sclerosis: A population based study. Amyotroph Lateral Scler 11, 439–442 (2010). [PubMed: 20225930]

69. Farace C, Fenu G, Lintas S, Oggiano R, Pisano A, Sabalic A, Solinas G, Bocca B, Forte G, Madeddu R, Amyotrophic lateral sclerosis and lead: A systematic update. NeuroToxicology 81, 80–88 (2020). [PubMed: 32941938]

70. van Blitterswijk M, van Es MA, Hennekam EAM, Dooijes D, van Rheenen W, Medic J, Bourque PR, Schelhaas HJ, van der Kooi AJ, de Visser M, de Bakker PIW, Veldink JH, van den Berg LH, Evidence for an oligogenic basis of amyotrophic lateral sclerosis. Human Molecular Genetics 21, 3776–3784 (2012). [PubMed: 22645277]

71. Nakae S, Nambu A, Sudo K, Iwakura Y, Suppression of immune induction of collagen-induced arthritis in IL-17-deficient mice. J Immunol 171, 6173–6177 (2003). [PubMed: 14634133]

72. Limone F, Mitchell JM, Juan IGS, Smith JLM, Raghunathan K, Couto A, Ghosh SD, Meyer D, Mello CJ, Nemesh J, Smith BM, McCarroll S, Pietiläinen O, Nehme R, Eggan K, Efficient generation of lower induced Motor Neurons by coupling Ngn2 expression with developmental cues, 2022.01.12.476020 (2022).

73. Dobin A, Davis CA, Schlesinger F, Drenkow J, Zaleski C, Jha S, Batut P, Chaisson M, Gingeras TR, STAR: ultrafast universal RNA-seq aligner. Bioinformatics 29, 15–21 (2013). [PubMed: 23104886]

74. Butler A, Hoffman P, Smibert P, Papalexi E, Satija R, Integrating single-cell transcriptomic data across different conditions, technologies, and species. Nat Biotechnol 36, 411–420 (2018). [PubMed: 29608179]

75. Macosko EZ, Basu A, Satija R, Nemesh J, Shekhar K, Goldman M, Tirosh I, Bialas AR, Kamitaki N, Martersteck EM, Trombetta JJ, Weitz DA, Sanes JR, Shalek AK, Regev A, McCarroll SA, Highly Parallel Genome-wide Expression Profiling of Individual Cells Using Nanoliter Droplets. Cell 161, 1202–1214 (2015). [PubMed: 26000488]

76. Wickham H, Averick M, Bryan J, Chang W, McGowan LD, François R, Grolemund G, Hayes A, Henry L, Hester J, Kuhn M, Pedersen TL, Miller E, Bache SM, Müller K, Ooms J, Robinson D, Seidel DP, Spinu V, Takahashi K, Vaughan D, Wilke C, Woo K, Yutani H, Welcome to the Tidyverse. Journal of Open Source Software 4, 1686 (2019).

77. Weinreb C, Wolock S, Klein AM, SPRING: a kinetic interface for visualizing high dimensional single-cell expression data. Bioinformatics 34, 1246–1248 (2018). [PubMed: 29228172]

78. Chen J, Kostenko V, Pioro EP, Trapp BD, MR Imaging-based Estimation of Upper Motor Neuron Density in Patients with Amyotrophic Lateral Sclerosis: A Feasibility Study. Radiology 287, 955–964 (2018). [PubMed: 29361242]

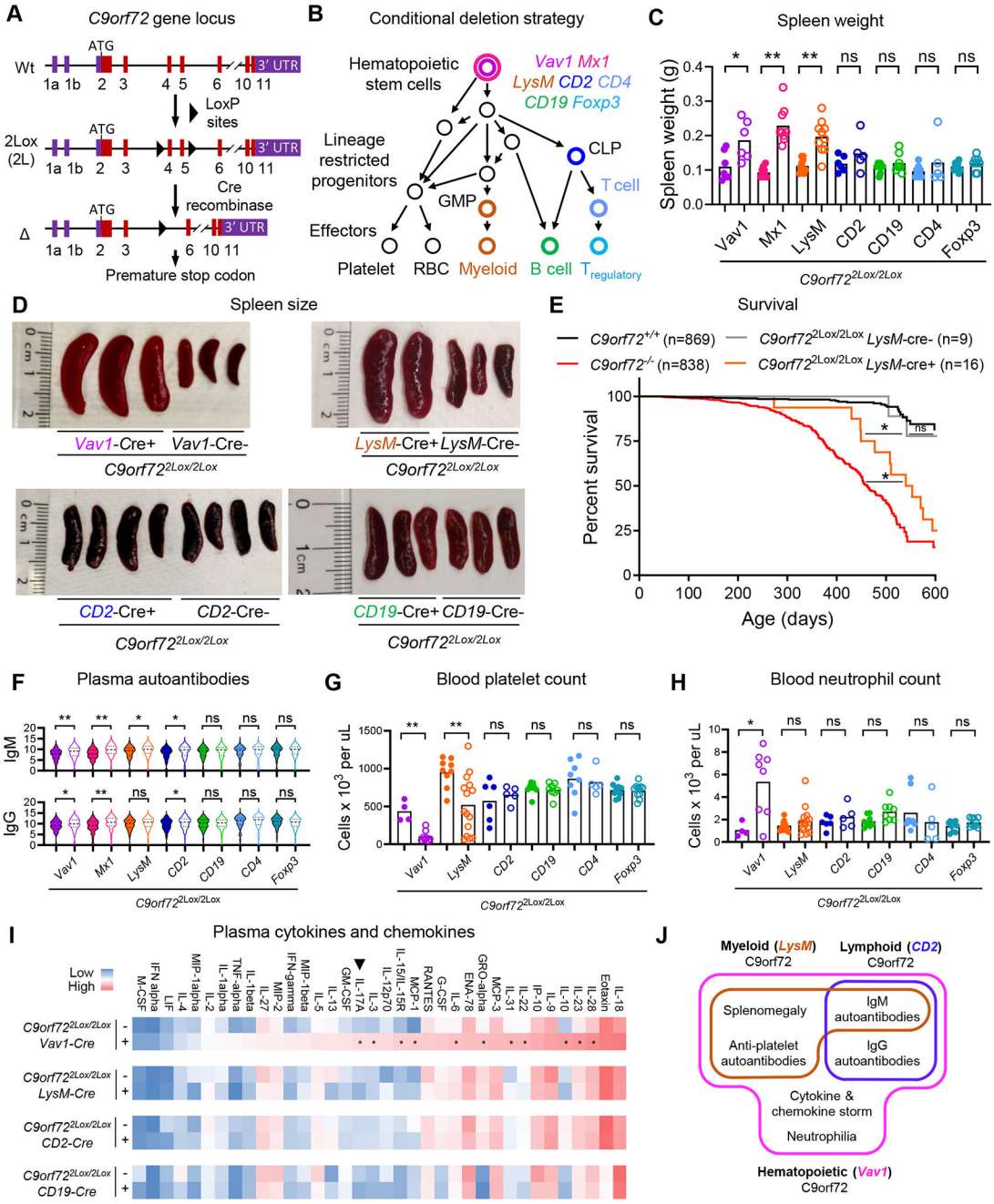

Fig. 1. *C9orf72* in myeloid and lymphoid lineages opposes autoimmunity and IL-17A production.

(**A**) *C9orf72* gene locus schematic and conditional mutagenesis strategy. Wt: *C9orf72* endogenous allele; 2Lox (2L): LoxP sites flanking exon 4-5; Δ: Cre-recombined allele with premature stop codon. (**B**) Hematopoietic stem and progenitor populations targeted for Cre recombination (*Vav1*: hematopoietic; *Mx1*: myeloid & lymphoid; *LysM*: myeloid; *CD2*: lymphoid; *CD4*: $CD4^+$ and $CD8^+$ T cells; *CD19*: B cells; *Foxp3*: T_{reg} cells). (**C**) Spleen weight of the following genotypes: 5-month-old *Vav1*-Cre− (n=7 per group) or *Vav1*-Cre+ (n=6 per group); 4-month-post-poly(I:C) *Mx1*-Cre− (n=10 per group) or *Mx1*-Cre+ (n=9

per group); 9-month-old *LysM*-Cre− (n=10 per group) or *LysM*-Cre+ (n=10 per group); 12-month-old *CD2*-Cre− (n=6 per group) or *CD2*-Cre+ (n=5 per group); 11-month-old, *CD19*-Cre− (n=8 per group) or *CD19*-Cre+ (n=8 per group); 15-month-old, *CD4*-Cre− (n=8 per group), *CD4*-Cre+ (n=5 per group); 11-month-old, *Foxp3*-Cre− (n=10 per group), *Foxp3*-Cre+ (n=8 per group); Each dot represents one mouse (Cre− controls filled, Cre+ open); data were analyzed by unpaired Student's t-test (*Vav1*, L*ysM, CD2, CD4, Foxp3*) or Mann-Whitney test (*Mx1, CD19*) between Cre+ and Cre− mice within each strain. (**D**) Spleens from mice with conditional deletion of *C9orf72* in the indicated lineages. (**E**) Survival of mice reared at Harvard University facility during the same two-year period. Animals that met pre-defined euthanasia criteria were considered a lethal event. $C9orf72^{+/+}$ and $C9orf72^{-/-}$ mice euthanized for reasons unrelated to the pre-defined criteria were censored at time of euthanasia; data were analyzed by Gehan-Breslow-Wilcoxon test. (**F to I**) Peripheral blood analysis of male and female mice evaluated in the following animals: 5-month-old *Vav1*-Cre− (n=4-9 per group) or *Vav1*-Cre+ (n=6-11 per group); 4-month post-poly(I:C) *Mx1*-Cre− or *Mx1*-Cre+ (n=9 per group); 9-month-old *LysM*-Cre− (n=6-9 per group) or *LysM*-Cre+ (n=7-15 per group); 12-month-old *CD2*-Cre− (n=5-8 per group) or *CD2*-Cre+ (n=4-10 per group); 11-month-old, *CD19*-Cre− (n=8-11 per group) or *CD19*-Cre+ (n=6-8 per group); 15-month-old, *CD4*-Cre− (n=8 per group), *CD4*-Cre+ (n=5 per group); 11-month-old, *Foxp3*-Cre− (n=4-10 per group), *Foxp3*-Cre+ (n=3-8 per group). Cre− (filled dot) and Cre+ (unfilled dot) mice are shown for each genotype. Plasma IgM and IgG autoantibodies against 124 self-antigens (**F**); data were analyzed by Mann-Whitney test. Blood platelet counts (**G**); data were analyzed by Student t-test (*LysM, CD2, CD19, Foxp3*) or Mann-Whitney test (*Vav1, CD4*). Blood neutrophil counts (**H**); data were analyzed by Student t-test (*Vav1, LysM, CD2, CD19, Foxp3*) or Mann-Whitney test (*CD4*). (**I**) Heatmap of individual plasma cytokine concentrations; arrowhead points to IL-17A, color normalized from low (blue) to high (red); data were analyzed by two-way ANOVA with Sidak's correction for multiple comparisons. (**J**) Summary of phenotypes in *C9orf72* conditional mutant mice. For all panels: * $p < 0.05$, ** $p < 0.01$, ns: not significant.

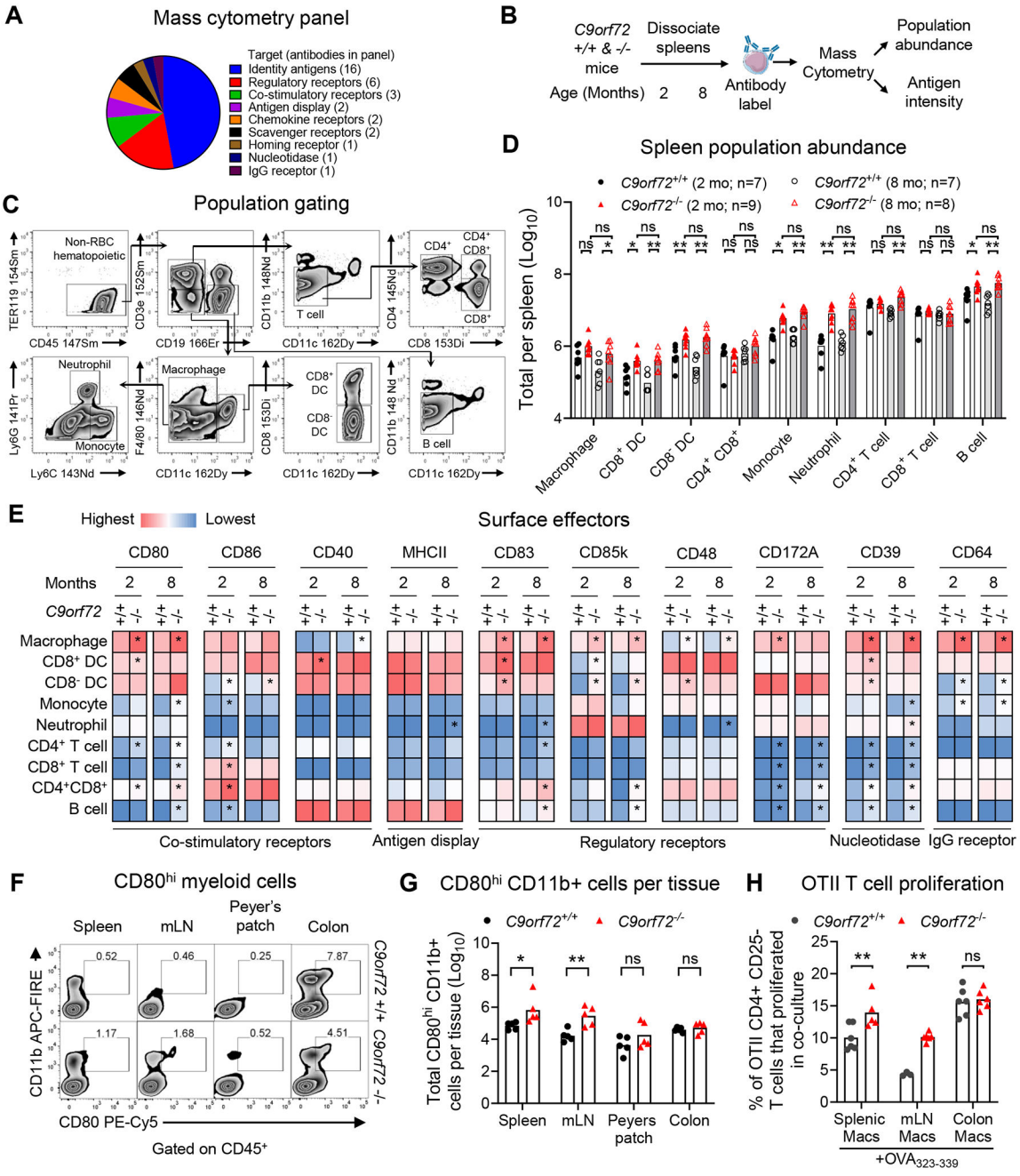

Fig. 2. Macrophage-expressed *C9orf72* restrains CD80 co-stimulation.

(**A**) Classification of antibody targets in mass cytometry panel. (**B**) Mass cytometry workflow from spleen of male and female littermates at 2- or 8-months of age. (**C**) Gating scheme of 9 defined splenocyte populations. (**D**) Cellular abundance of each gated population from spleen. Dendritic cell (DC). 2mo: *C9orf72*$^{+/+}$ (n=7 per group); *C9orf72*$^{-/-}$ (n=9 per group); 8mo: *C9orf72*$^{+/+}$ (n=7 per group); *C9orf72*$^{-/-}$ (n=8 per group), dots represent individual mice; data were analyzed by one-way ANOVA with Sidak's correction for multiple comparisons (Macrophage, CD8^{-} DC) or Kruskal-Wallis test with Dunn's

correction for multiple comparisons ($CD8^+$ DC, $CD4^+CD8^+$T, Monocyte, Neutrophil, $CD4^+$T, $CD8^+$T, B cell). (**E**) Average effector median staining intensity on surface of gated splenic populations. For each effector, color scale was normalized from lowest (blue) to highest (red) expression across populations. Data were analyzed by Student's t-test or Mann-Whitney test with Bonferroni's correction for multiple comparisons, * $p < 0.0056$. (**F**) Representative flow cytometry plots of CD11b and CD80 among $CD45^+$ cells in the indicated tissues from *C9orf72*$^{+/+}$ (top) or *C9orf72*$^{-/-}$ (bottom). mLN, mesenteric lymph node. (**G**) Quantification of $CD11b^{hi}$ $CD80^+$ cells in the indicated tissues; dots represent individual mice; data analyzed by two-way ANOVA with Sidak's correction for multiple comparisons. (**H**) Percentage of OTII T cell receptor transgenic T cells with diluted carboxy fluorescein succinimidyl ester (CFSE) signal after 4 days in co-culture with tissue enriched Ovalbumin (OVA) peptide-loaded macrophages; dots represent individual wells; data were analyzed by two-way ANOVA with Sidak's correction for multiple comparisons. Unless otherwise stated, * $p < 0.05$, ** $p < 0.01$, ns. not significant.

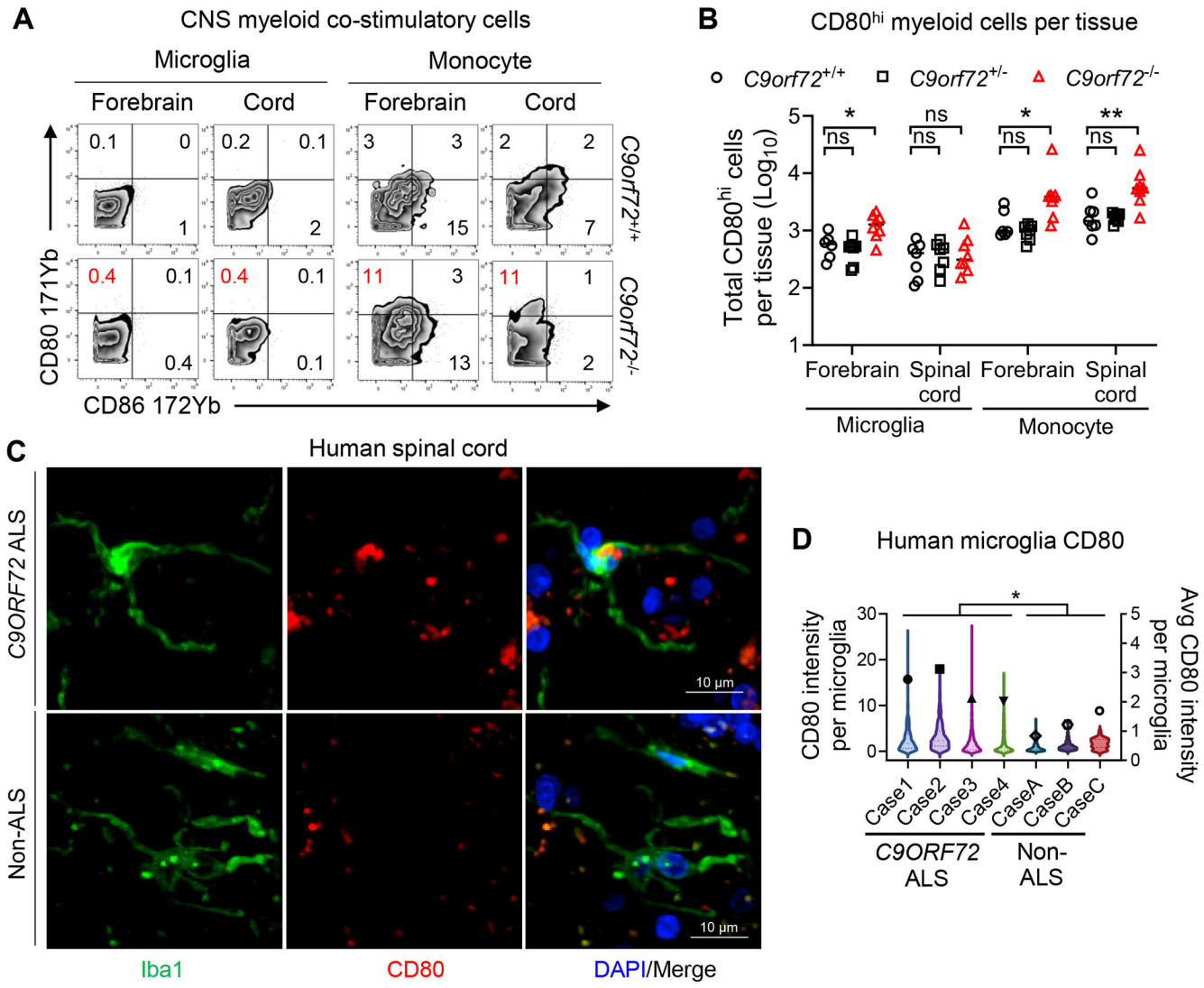

Fig. 3. CD80 is enriched in microglia from *C9orf72*$^{-/-}$ mice and patients with *C9ORF72* ALS.

(**A and B**) Mass cytometry of forebrain and spinal cord of male and female littermates at 8 months of age (*C9orf72*$^{+/+}$, n=7; *C9orf72*$^{+/-}$, n=7; *C9orf72*$^{-/-}$, n=8). One *C9orf72*$^{+/+}$ forebrain sample was excluded due to failed tissue isolation. (**A**) Representative CD80 and CD86 expression in microglia (left, CD45^{mid} CD11b^{+} CD39^{+} CX3CR1^{+}) and monocytes (right, CD45^{hi} CD11b^{+} Ly6C^{+}). Numbers on plots represent percent of the gated population. (**B**) Abundance of each gated population. Each dot represents one animal; data were analyzed by one-way ANOVA with Dunnett's correction for multiple comparisons. (**C**) Representative human spinal cords stained for Iba1 (green), CD80 (red), and DAPI (blue); scale 10µm. (**D**) CD80 intensity per Iba1^{+} human spinal cord microglia with n > 440 microglia imaged per case (left axis, violin plot). Overlaid dot represents the average microglia CD80 intensity per case (right axis). Data were analyzed by unpaired Student's t-test of average microglia CD80 intensity between *C9ORF72* ALS cases (n=4) and non-ALS controls (n=3). For all panels: * $p < 0.05$, ** $p < 0.01$, ns. not significant.

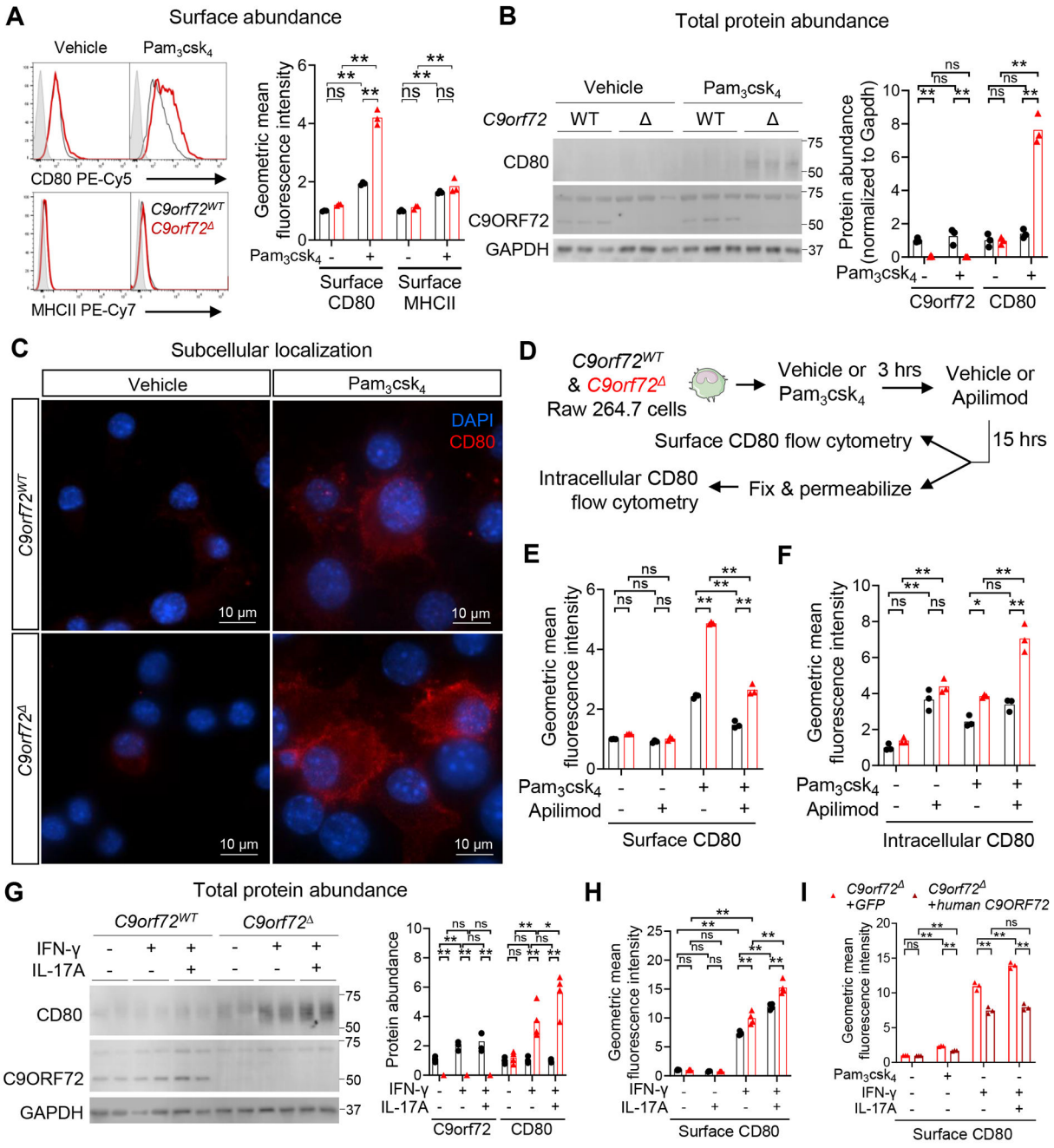

Fig. 4. *C9orf72* governs CD80 trafficking in response to TLR agonist and cytokine exposure.

CRISPR/Cas9-edited Raw 264.7 murine macrophage cells with intact (*C9orf72*^{WT}) or LOF mutated (*C9orf72*^{Δ}) *C9orf72* locus were used for *in vitro* studies in all panels. Each dot represents one well. (**A**) Surface antibody staining and flow cytometry for CD80 or MHCII after 18hr exposure to vehicle or TLR2 agonist Pam_3csk_4. (**B**) Whole cell lysate western blot and densitometry quantification analysis 18hrs after exposure to vehicle or Pam_3csk_4. (**C**) Immunofluorescent staining for CD80 (red) after 18hr exposure to vehicle or Pam_3csk_4. (**D**) Experimental design with PIKFyve lipid kinase inhibitor Apilimod to disrupt vesicle

trafficking. (**E**) Surface or (**F**) intracellular CD80 staining intensity by flow cytometry. (**G**) Whole cell lysate western blot and quantification after 18hr exposure to vehicle or recombinant murine IFN-γ with or without recombinant murine IL-17A. (**H**) Surface antibody staining for CD80 and flow cytometry after 18hr vehicle or cytokine exposure. (**I**) *C9orf72*$^{\Delta}$ cells transfected with GFP or human *C9ORF72* expression plasmid 2 days before 18hr stimulation, surface staining for CD80 and analysis by flow cytometry. Each dot represents one replicate; all experiments were repeated at least twice; data were analyzed by two-way ANOVA with Sidak's correction for multiple comparisons; * $p < 0.05$. ** $p < 0.01$. ns. not significant.

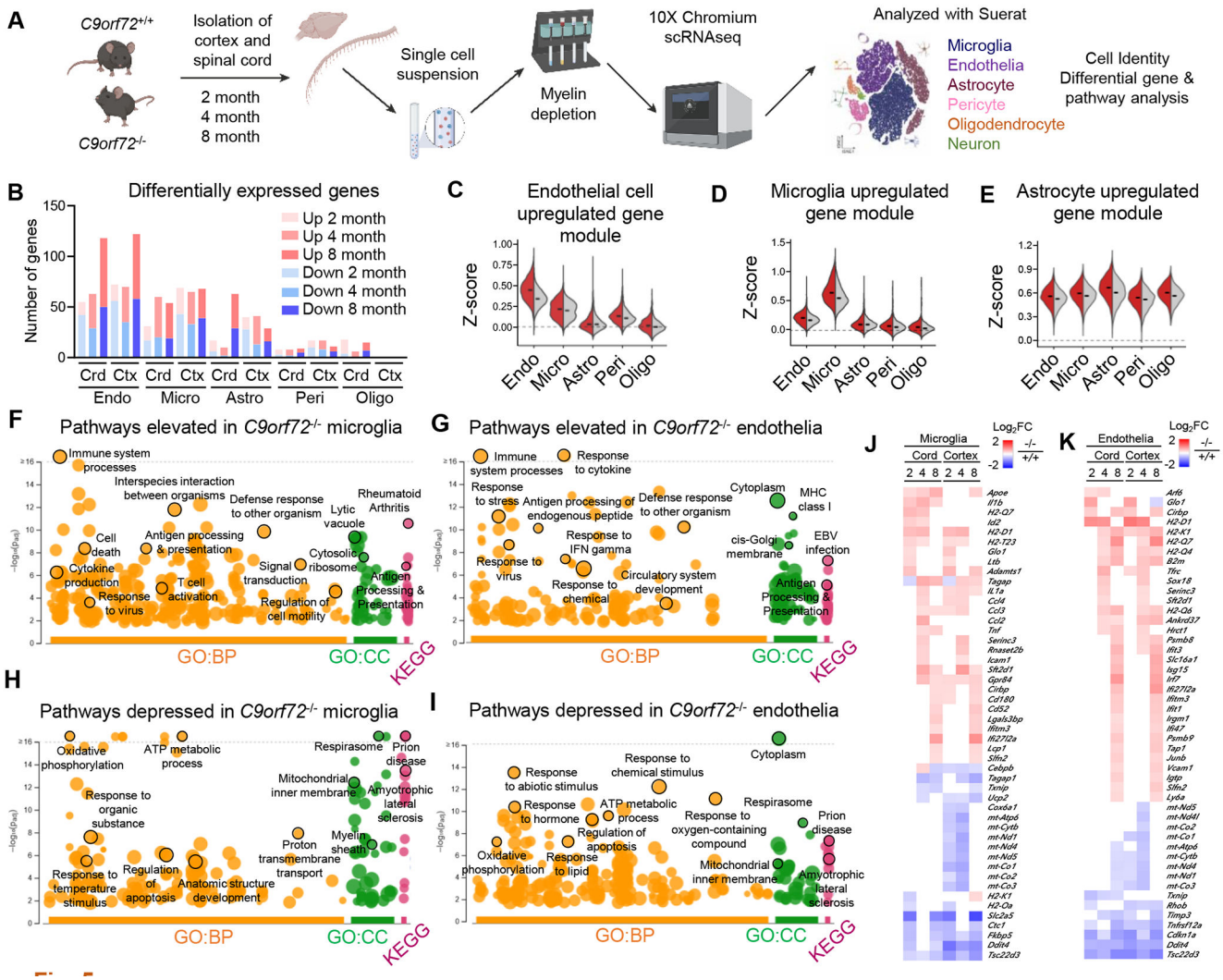

Fig. 5. *C9orf72*$^{-/-}$ microglia and endothelial cells exhibit a coordinated inflammatory gene profile.

(**A**) Single cell RNA sequencing workflow from spinal cord and brain cortex at 2, 4 and 8 months of age in female *C9orf72*$^{+/+}$ (n=3) and *C9orf72*$^{-/-}$ (n=3) littermates. (**B**) Total number of genes differentially expressed (adjusted $p < 0.05$) between *C9orf72*$^{+/+}$ and *C9orf72*$^{-/-}$ populations. Up-regulated genes are red, down-regulated genes are blue. Abbreviations include endothelia (Endo), microglia (Micro), astrocyte (Astro), pericyte (Peri), oligodendrocyte (Oligo), spinal cord (Crd), brain cortex (Ctx). (**C to E**) Module score of genes upregulated in endothelial cells (**C**), microglia (**D**), or astrocytes (**E**) across *C9orf72*$^{-/-}$ (red) and *C9orf72*$^{+/+}$ (gray) populations. (**F and G**) gProfiler pathway enrichment based on genes increased in *C9orf72*$^{-/-}$ (**F**) microglia or (**G**) endothelial cells. (**H and I**) gProfiler pathway enrichment based on genes decreased in *C9orf72*$^{-/-}$ (**H**) microglia or (**I**) endothelial cells. Gene Ontology (GO); Biological Pathways (BP); Cell Compartment (CC); Kyoto Encyclopedia of Genes and Genomes (KEGG). (**J**) Genes differentially expressed between *C9orf72*$^{+/+}$ and *C9orf72*$^{-/-}$ microglia in spinal cord and

cortex by age. (**K**) Genes differentially expressed between *C9orf72*$^{+/+}$ and *C9orf72*$^{-/-}$ endothelial cells in spinal cord and cortex by age.

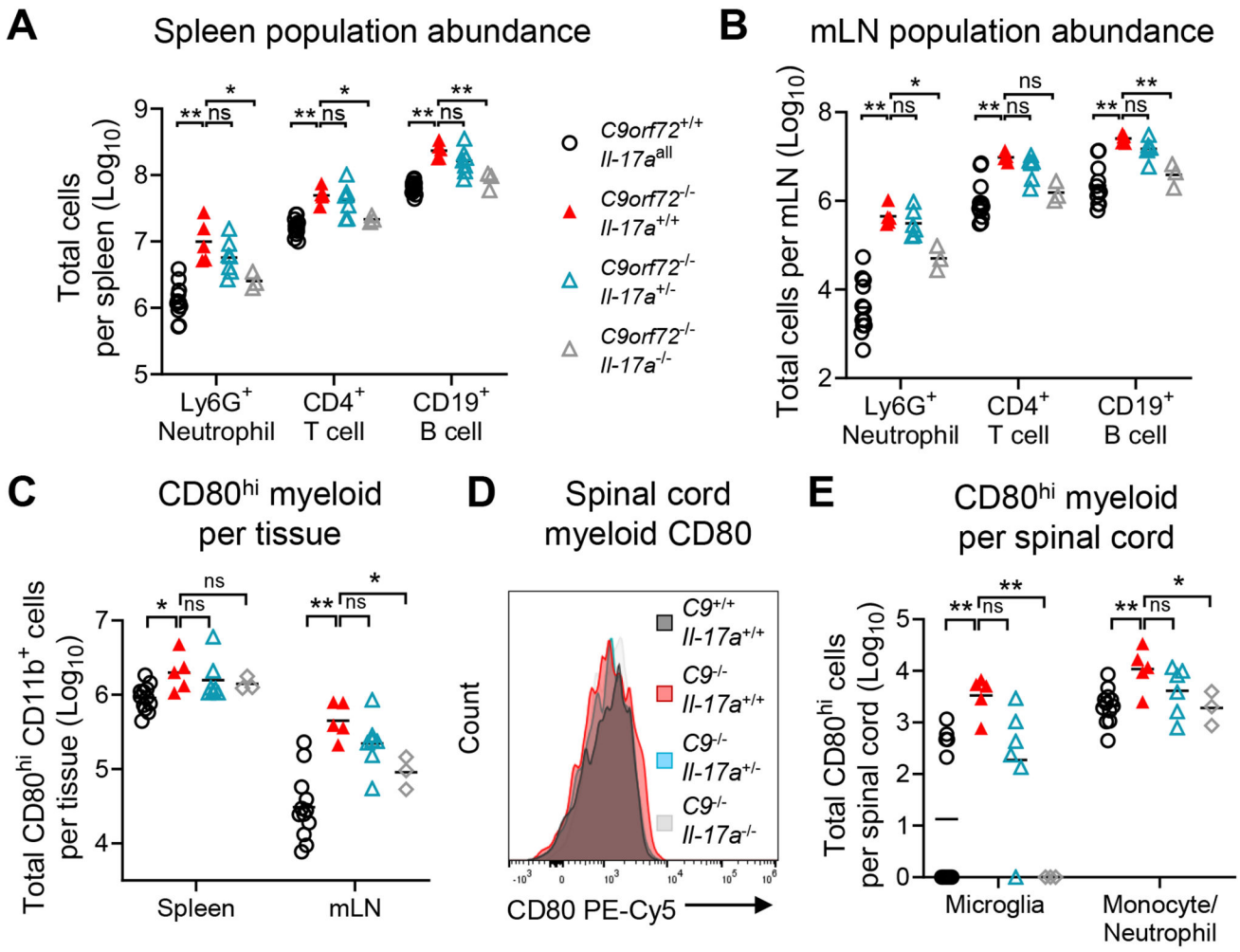

Fig. 6. *Il-17a* deficiency reduces CD80 expression in *C9orf72*$^{-/-}$ gut and spinal cord.

(**A to C**) Cellular abundance of each gated population at 6 months of age. (**A**) Ly6G^{+} Neutrophil, CD4^{+} T cell, and CD19^{+} B cell abundance per spleen. (**B**) Ly6G^{+} Neutrophil, CD4^{+} T cell, and CD19^{+} B cell abundance per mLN. (**D**) Spleen and mLN CD11b^{+} CD80^{hi} cell abundance. (**E**) Representative surface staining of CD80 on CD11b^{+} spinal cord cells. (**F**) Spinal cord CD45^{mid} CD11b^{+} CD80^{hi} microglia and CD45^{hi} CD11b^{+} CD80^{hi} monocyte/neutrophil abundance. *C9orf72*$^{+/+}$ *Il-17a*$^{+/+}$ (n=4 per group); *C9orf72*$^{+/+}$*Il-17a*$^{+/-}$ (n=4 per group); *C9orf72*$^{+/+}$ *Il-17a*$^{-/-}$ (n=4 per group); *C9orf72*$^{-/-}$ *Il-17a*$^{+/+}$ (n=5 per group); *C9orf72* $^{-/-}$ *Il-17a* $^{+/-}$ (n=7 per group); *C9orf72* $^{-/-}$ *Il-17a* $^{-/-}$ (n=3 per group) with sexes combined. One *C9orf72*$^{-/-}$ *Il-17a*$^{+/-}$ spinal cord sample was excluded due to failed isolation of cells within it; each dot represents one mouse; horizontal bars represents mean; data were analyzed by one-way ANOVA with Dunnett's correction multiple comparisons within spleen Neutrophil, CD4^{+}, B cell, mLN Neutrophil, B cell, CD80^{hi} CD11b^{+} and spinal cord CD45^{hi} CD11b^{+} CD80^{hi} monocyte/neutrophil or Kruskal-Wallis test with Dunn's multiple comparisons within spleen CD80^{hi} CD11b^{+}, mLN CD4^{+} and spinal cord CD45^{mid} CD11b^{+} CD80^{hi} microglia ; * $p < 0.05$, ** $p < 0.01$, ns. not significant.

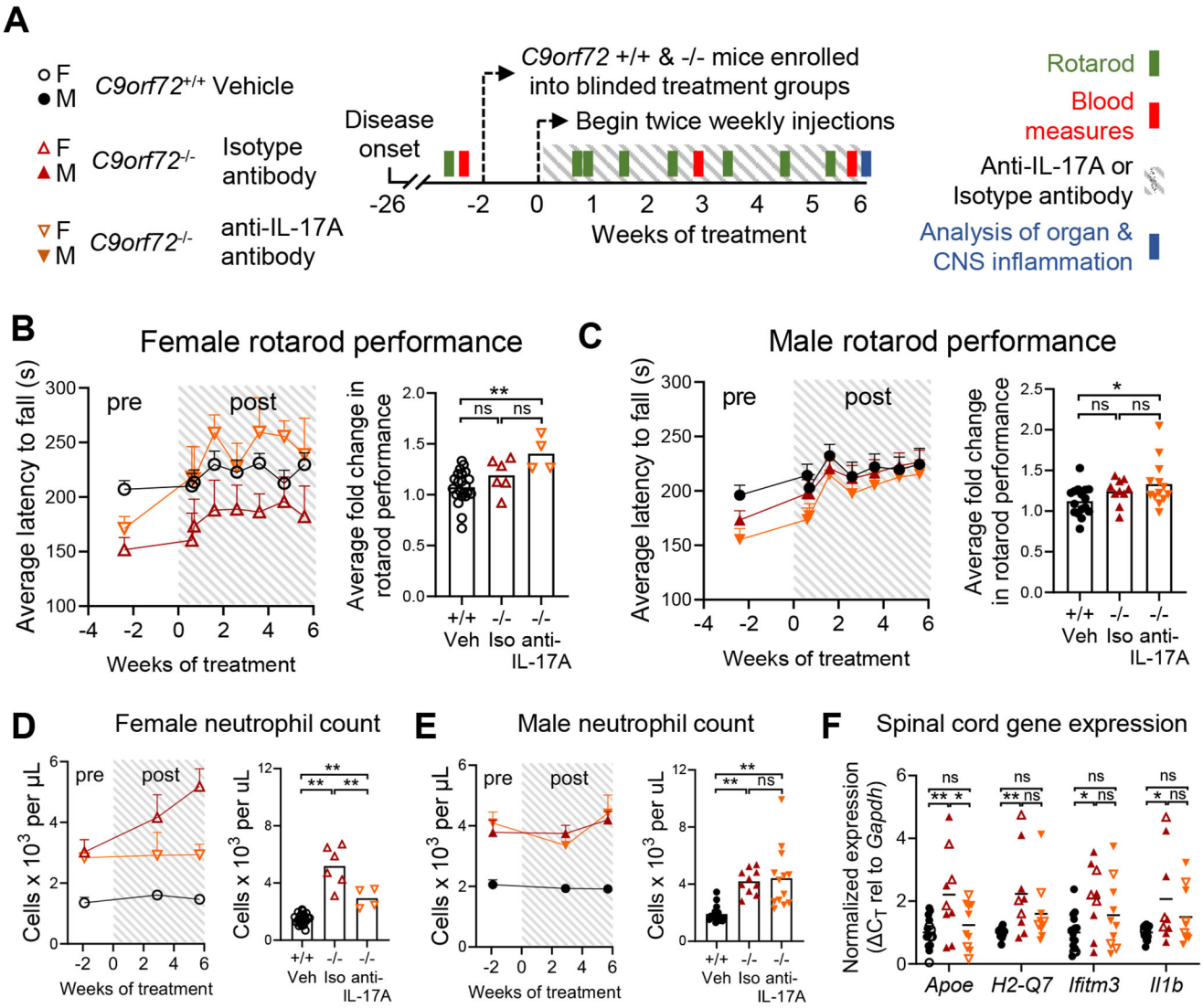

Fig. 7. Therapeutic neutralization of IL-17A improves motor performance in *C9orf72*$^{-/-}$ mice.

(**A**) Study design with female (open symbol) and male (closed symbol) *C9orf72*$^{+/+}$ (n=22 female and n=16 male) and *C9orf72*$^{-/-}$ (n=11 female and n=25 male) mice. Treatment groups included *C9orf72*$^{+/+}$ mice treated with vehicle (n=38), *C9orf72*$^{-/-}$ mice treated with isotype control antibody (n=6 female and n=12 male; n=2 males not assessed due to premature mortality) and *C9orf72*$^{-/-}$ mice treated with anti-IL-17A antibody (n=5 female and n=13 male; n=1 female not assessed due to premature mortality). (**B and C**) Rotarod performance of (**B**) females and (**C**) males over study duration. Data presented as mean ± SEM. For bar plots, each dot represents average fold change in performance of individual mice over 6 weeks relative to pre-treatment; data were analyzed by one-way ANOVA with Tukey's correction for multiple comparisons. (**D and E**) Neutrophil count in peripheral blood of (**D**) females and (**E**) males over study duration. For bar plots, each dot represents individual mice at week 6 time point; data were analyzed by (**D**) one-way ANOVA with Tukey's correction for multiple comparisons and (**E**) Kruskal-Wallis test with

Dunn's correction for multiple comparisons. (**F**) Normalized gene expression of single cell dissociated myelin-depleted spinal cord cells evaluated in the following animals: *C9orf72*$^{+/+}$ mice treated with vehicle (n=6 female and n=9 male), *C9orf72*$^{-/-}$ mice treated with isotype control antibody (n=3 female and n=6 male) and *C9orf72*$^{-/-}$ mice treated with anti-IL-17A antibody (n=3 female and n=7 male). Each dot represents one mouse; horizontal bar represents mean; data were analyzed by two-way ANOVA with Tukey's correction for multiple comparisons; for all panels: * $p < 0.05$, ** $p < 0.01$, ns. not significant.